European Journal of Pharmaceutics and Biopharmaceutics 71 (2008) 2–22

Contents lists available at ScienceDirect

European Journal of Pharmaceutics and Biopharmaceutics

journal homepage: www.elsevier.com/locate/ejpb

Review article

In-vitro tomography and non-destructive imaging at depth of pharmaceutical solid dosage forms

J. Axel Zeitler *, Lynn F. Gladden

Department of Chemical Engineering and Biotechnology, University of Cambridge, Cambridge CB2 3RA, UK

ARTICLE INFO

Article history:
Received 16 May 2008
Accepted in revised form 13 August 2008
Available online 22 August 2008

Keywords:
Solid dosage form
Tomography
Non-destructive testing
Process analytical technology (PAT)
Controlled release
X-ray microtomography
Magnetic resonance imaging (MRI)
NMR imaging
NMR microscopy
Terahertz pulsed imaging (TPI)
Optical coherence tomography (OCT)

ABSTRACT

Tomographic imaging techniques offer new prospects for a better understanding of the quality, performance and release mechanisms of pharmaceutical solid dosage forms. It is only over the last fifteen years that tomography has been applied for the *in-vitro* characterisation of dosage forms. This review aims to introduce the concept of tomography in a pharmaceutical context, and describes the current state-of-the-art of the four most promising techniques: X-ray computed microtomography, magnetic resonance imaging, terahertz imaging and optical coherence tomography. The basic working principles of the techniques are introduced and the current pharmaceutical applications of the technologies are discussed, together with a comparison of their specific strengths and weaknesses. Possible future developments in these fields are also discussed.

1. Introduction

Along with the recent breakthroughs in photonics – focal plane array detectors, optical fibres and compact lasers operating over a range of frequencies, to name a few – spectroscopic imaging techniques, in particular at infrared frequencies, have featured prominently in pharmaceutical formulation research over the last decade. The ability to perform spatially resolved investigations of molecular interactions in the formulation, during processing and in the final dosage form, has led to a better understanding of pharmaceutical processing steps and the resulting dosage form [1–4]. This development highlights one of the advantages that can be achieved simply by transforming a spatially unresolved spectroscopic experiment to a spectroscopic image.

The recent interest in process analytical technology (PAT) was catalysed by a number of initiatives on the regulatory level: the FDA's initiative to transform the pharmaceutical cGMP regulations towards a more risk-based framework; the ICH guidelines Q8, Q9 and Q10 focusing on quality by design (QbD) as the new paradigm in pharmaceutical development and production, and the initiative by the EMEA to implement PAT submission procedures and real-time release. All these developments have led to a strong demand for fast acquisition spectroscopic techniques. The focus on vibrational spectroscopy for PAT can be explained by the combination of rich information content provided by the spectra and simultaneous developments in technology, i.e. well developed waveguides such as optical fibres that allow the construction of spectroscopic probes for real-time processing applications in-line, on-line and at-line in a manufacturing facility along with both robust and affordable instrumentation [5,6]. The motivation for all initiatives that have evolved around PAT is to use the data acquired from in-line sensors to subsequently control the process, and thus achieve a better quality product based on the – ideally full scientific – understanding that has been built up during the product development phase. It is therefore quintessential to understand, on a fundamental level, which properties during the process have what impact on the final product in order to predict changes of the quality of the dosage form as a result of changes in the processing conditions. Once this understanding is established a successful process control loop can be designed and implemented.

Most commonly, the quality of the finished solid dosage form is assessed using basic parameters such as the spatial dimensions of the dosage form, its hardness, mass, content uniformity, porosity, friability, tensile strength, moisture content, disintegration time,

* Corresponding author. Department of Chemical Engineering and Biotechnology, University of Cambridge, Pembroke Street, Cambridge CB2 3RA, UK, Tel.: +44 1223 761631; fax: +44 1223 334796.
E-mail address: jaz22@cam.ac.uk (J.A. Zeitler).
URL: http://www.pssrc.org (J.A. Zeitler).

0939-6411/$ - see front matter © 2008 Elsevier B.V. All rights reserved.
doi:10.1016/j.ejpb.2008.08.012

dissolution profile and the weight gain during coating. All these traditional parameters are well established in the modern pharmacopoeias, and have served for a long time as benchmarks during the dosage form development process. However, while they are an integral part of modern PAT development and process control, they lack specificity and/or spatial resolution and lead to an insufficient basis for the full understanding of the dosage form. Even though tight specifications are in place to monitor the quality of the final products, each year a number of dosage forms fail after approval, and have to be recalled from the market. In 2007 alone, approximately sixty recalls were documented for pharmaceutical tablets in the FDA enforcement report for the United States. About 30% of these recalls were due to wrong labels or packaging, while recalls due to problems with dissolution/disintegration, impurities or content each attributed for about 20% of the recalls [7]. These numbers only cover dosage forms that have initially passed the quality control specifications and were released on the market. The number of failed batches that are produced and have to be discarded immediately after production due to their poor quality is estimated to be orders of magnitude higher.

While a number of techniques have been successfully introduced to pharmaceutical research and development in order to investigate fundamental properties of a formulation on the molecular, particular and particle ensemble level, the present research activities and instrumentation on the level of the entire dosage form itself are somewhat less developed. With the advent of more complex dosage forms, there is a need to fully characterise and understand the performance limiting properties of such dosage forms. Even though processing technology has advanced considerably over the last decade, the fundamental understanding of the processing steps is not yet fully developed, and it is this lack of understanding which is the reason for the failure of some such products in recent years.

This review focuses on four techniques that have the potential to provide the required tools: X-ray computed microtomography (XμCT), magnetic resonance imaging (MRI), imaging at terahertz frequencies and optical coherence tomography (OCT). Rather than being confined to information from the surface of the dosage forms all four techniques can be considered tomographic techniques, which means that they are able to non-destructively resolve the three-dimensional structure of the dosage form. In this context, tomography is defined as the "cross-sectional imaging of an object from either transmission or reflection data collected by illuminating the object from many different directions" [8]. MRI is considered to be a tomographic technique in the context of this review even though the three-dimensional imaging methodology is not necessarily associated with the reconstruction of two-dimensional cross-sectional images. In addition to their ability to provide non-destructive tomographic information, all four techniques are able to resolve the internal structure of typical pharmaceutical excipients that are opaque at visible frequencies. Other imaging techniques that can also image at depth, such as confocal imaging [9], are not a part of this review as they have only a limited ability to penetrate typical excipients used for the formulation of pharmaceutical solid dosage forms. Techniques that require large central facilities such as synchrotrons are also excluded from consideration.

2. Computed tomography

2.1. Introduction to computed tomography

In contrast to a two-dimensional projection image, which is typically acquired by propagating a collimated beam either through the object of interest or by reflecting it off its surface at normal incidence, a full three-dimensional image is not recorded directly but is obtained through reconstruction of two-dimensional image cross-sections and subsequent stacking of the reconstructed slices.

In traditional computed tomography (CT), data for one slice in the *xy* plane are acquired at different angles, the object is moved in the *z*-direction and the process is repeated until the area of interest has been covered. The corresponding slices are reconstructed, and a three-dimensional image is obtained by stacking all slices on top of one another. In this approach the resolution in the *z*-direction is mainly limited by the beam diameter, the dimensions of the detector and scattering of the radiation.

The slice images are reconstructed by mathematical algorithms using a number of projections at different angles through the sample in the *xy* plane. The projections can be acquired in transmission, reflection or from scattered radiation; however, for clarity the remainder of this section will only discuss tomography in transmission. Further details of the development of computed tomography and the image reconstruction techniques can be found in Section 1.1 in the electronic supplementary material.

A further important advancement in CT was achieved by the development of setups that are capable of providing three-dimensional images without the need for acquiring sequences of two-dimensional slices and subsequent stacking of the slices. This was realised by using a diverging cone-beam rather than a two-dimensional fan or collimated beam together with a scintillator screen coupled to a 2D CCD detector array for detection (see the next section for details). The image reconstruction requires the implementation of algorithms such as the Feldkamp algorithm [10], which is capable of reconstructing the three dimensional image from the cone-beam data. The details of the reconstruction techniques are out of the scope of this article and the reader is referred to the literature [11,12,8].

Even though computed tomography is most frequently employed using X-rays, the principle of tomographic image reconstruction can be applied over the whole range of the electromagnetic spectrum as long as the radiation can, at least partially, penetrate the object of interest. Due to their high energy, X-rays have the advantage of being able to penetrate easily all pharmaceutically relevant excipients, exhibit negligible diffraction and as a consequence of the short wavelength allow for very high resolution images. However, tomography with X-rays will not always be the method of choice to investigate the internal structure of solid dosage forms. The image contrast is dependent on either relatively high density differences in the material, which often is not the case for a standard tablet, or the presence of atoms with different mass, which again is not necessarily common. In cases where X-rays do not lead to sufficient contrast it can be advantageous to use different types of radiation to acquire tomographic images. Examples of such experiments will be introduced later in this review.

2.2. X-ray microtomography (XμCT)

X-ray microtomography (XμCT) was evolved from medical CT with the aim to image small objects with high resolution. In 1982, the principle of XμCT was first demonstrated by Elliott and Dover [13] by an example of a tomographic image through the shell of a freshwater snail on a setup similar to a CT scanner used by Hounsfield. In this experiment the spatial resolution of the reconstructed cross-section was better than 20 μm. There is no clear distinction at what resolution the conventional CT ends and where XμCT starts but it is suggested that any results with higher spatial resolution than 100 μm should be regarded as XμCT [14].

In contrast to conventional CT, where X-ray source and detector are rotated around the sample object, the equipment used for modern XμCT typically rotates the sample object while source and

detector are kept stationary (Fig. 1). Starting from the experimental setups used by Elliott and Dover, more advanced instruments have been developed that use a collimated beam of X-rays combined with a matching 2D array detector [15]. By restricting the dimensions of the sample object to sizes smaller than the diameter of the X-ray beam, such systems are able to acquire tomographic data of whole 3D objects in one rotation scan without the need for iterating the sample in z direction after the acquisition of a single xy slice. Unfortunately, only synchrotron facilities provide bright enough light sources for the operation of these parallel beam setups.

Almost all experimental work on XμCT which has been published in the pharmaceutical field is performed on instruments that use a cone beam in combination with a 2D array detector. As in the parallel beam setups, it is possible to image a whole three-dimensional object by just rotating the object through 180° and recoding the projection images using the cone-beam configuration. Higher resolutions have been acheived through the development of X-ray tubes with very small apertures providing point-like sources. The major limitation of these setups is that there is a trade-off between sample size and magnification. The shadow of the projected object must not exceed the field of view on the detector. In order to achieve magnifications of 120× and higher, the object has to be restricted to a maximum size of about 2 mm. A further disadvantage of instruments based on the setup shown in Fig. 1 is that they are inherently susceptible to ring artefacts. This is due to the fact that each detector element is used for the same projection in all shadow images and subtle differences in the sensitivity between the individual array elements, which are unavoidable in CCDs, will lead to ring artefacts in the reconstructed images.

One elegant solution to overcome both problems is to use time-delay integration methods as introduced by Davis and Elliott [16]. The same authors have also published a very clear overview about the different types of artefacts in XμCT [17] and how to use the technique quantitatively for chemical element analysis [18]. Stock has provided an excellent comprehensive review of XμCT in a materials science context, and the reader is referred to this review for more details on the technique [14]. A first thorough overview of pharmaceutical applications for XμCT was compiled by Hancock and Mullarney [19].

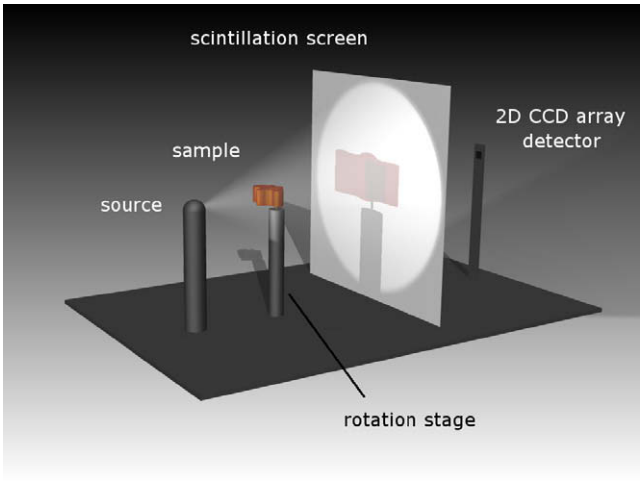

Fig. 1. Cone-beam XμCT setup. A point source emits a diverging beam of X-rays. The X-rays penetrate the sample object and are attenuated. The transmitted radiation, or shadow image, of the object is projected onto a scintillation screen which typically uses a layer of phosphor to convert the X-rays to visible light. Optical lenses or fibre optics coupled to the scintillator (not shown) are used to project the image from the scintillation screen to a 2D CCD array detector. After the shadow image is acquired the object is rotated. The magnification is set by adjusting the distance between the sample object and the X-ray source. The maximum magnification is limited in that for all angles θ the shadow of the object must not exceed the size of the scintillation screen.

2.3. Pharmaceutical applications

The work by Farber, Tardos and Michaels on the porosity and morphology of granules is the first example of XμCT being used in a pharmaceutical context [20]. The results for the porosity measurements by XμCT were compared to mercury porosimetry and gas absorption measurements. However, the resolution of the measurement is limited to pores bigger than 4 μm. The pore size distribution is also strongly dependent on the contrast between the pores and the material. As the density of typical pharmaceutical excipients is not very high, the contrast between the material and the air in the pores is not always unequivocal in the reconstructed images. In order to calculate the pore size, the images need to be converted from greyscale (different densities) to binary (material or air) images. During this process a threshold of what density is regarded as air and what as sample material has to be defined which has a very strong impact on the resulting pore size. The authors concluded that the precision of XμCT for the determination of pore sizes is inferior to mercury porosimetry, yet XμCT gives additional information in terms of the pore morphology, spatial distribution and connectivity. Furthermore, the true pore size distribution is obtained rather than only the size distribution of the pore "necks" as is the case in mercury porosimetry.

Ansari and Stepanek used XμCT for the characterisation of the granule microstructure during the development of a fluid bed melt granulation process [21]. They were able to show the formation of hollow core granules by XμCT depending on the formulation composition and particle size of the excipients used. Based on the results obtained by XμCT, they were able to develop a mathematical model to aid the formulation development.

Yang and Fu studied compaction and mixing processes of powders using XμCT [22]. For their study, Yang and Fu developed a lead labelling method to trace highly spherical microcrystalline cellulose (MCC) particles during compaction and blending experiments. The MCC particles were separated into different fractions and impregnated with varying amounts of lead (II) acetate trihydrate. Lead (atomic number 82) is strongly absorbing at X-ray energies, and the impregnation with the lead solution provides an excellent contrast between the different particle fractions. By tracing the relative positions and movements of the lead impregnated particles, die compaction and mixing in a model V-blender on the particulate level was investigated. The authors concluded from the compaction experiments that the local strains within one region of the compact are not identical with the global strain. In a miniature V-blender, Yang and Fu studied different mixing processes using two fractions of MCC particles, one labelled with lead acetate and the other fraction unlabelled. The particle size distribution for both fractions was identical. For the mixing experiments, the analysis was performed using the shadow images rather than reconstructed cross sections. Different loading configurations for the blender were investigated. It was possible to study the mixing process both qualitatively and quantitatively using 1D profiles. This is a valuable first step in developing XμCT for process applications. However, one arm of the model mixer used for the study only measures 18 mm, and the particles used for the study had a size of around 200 μm. Given the small scale of the mixer required for the XμCT experiments, it remains to be seen whether the results can be transferred to the conditions in an industrial mixer.

The first application of XμCT to investigate the entire pharmaceutical dosage forms is the study by Ozeki et al. [23]. Tomographic cross-sections of dry-coated tablets were used qualitatively in order to investigate differences in density between the different tablet components and to detect exfoliation between these structures.

At a compaction pressure of 100 MPa, the contrast between the tablet core and the dry coating was very weak, while it was much stronger at a compaction pressure of 200 MPa. No exfoliation was detected.

One of the early applications of XμCT in the materials science community was the measurement of density variations in compacts [24]. Following up on these studies, compaction of pharmaceutical powder mixtures was investigated. Sinka et al. used direct compressed tablets of different geometry and embossing made of MCC [25] to assess the applicability of XμCT for the quantitative measurement of density variations within tablets. The model tablets were compressed at two different compaction forces. Considerable density differences within the tablets were detected (Fig. 2).

Busignies et al. studied localised density variations in tablets of the form of flat faced cylindrical compacts of MCC by XμCT [26]. The tablets were compacted over a range of pressures between 40 and 280 MPa, and the linearity of the X-ray attenuation as a function of density was validated over the range of samples. The greyscale of the reconstructed image slices was calibrated to the material density, and this calibration was used to produce false-colour maps of the spatial density distribution within the tablets (Fig. 3A). Significant density variations within the tablets of more than 10% were detected. It was found that the tablets are denser at the surface compared to the centre, which was attributed to the wall friction during the compaction process. This effect was more pronounced with increasing compaction pressure. In addition, the thickness of the ring of higher density along the central band of the tablet was found to decrease with increasing compaction pressure (Fig. 3B). It was suggested that this property is important with regard to the friability of the tablet, in particular, when the tablet is embossed with structures at length scales comparable to the density gradient. The density distribution along the *z* axis was found to be much more uniform for the cylindrical model tablets studied.

Fu et al. investigated the packing structure in granular systems [27]. Two model systems of packed powders were used: glass beads and spherical MCC particles ranging from 180 to 300 μm in diameter. An algorithm was developed, and applied to reconstructed XμCT slices of both the systems, to automatically identify and locate the absolute position of individual particles in a three-dimensional coordinate system. The identification was based on the unique particle morphology, and thus no tracer particles were required for the experiments. The experimental results were found to be in quantitative agreement with simulations for the packing using a discrete element modelling (DEM) code.

In addition to the previous, study Fu et al. used the same approach to study the displacement of marker particles in a powder bed *in situ* during compaction [28]. For the experiments the authors designed a compression rig made of polycarbonate and flat faced metal punches that was suitable for *in situ* XμCT image acquisition. In this rig, only the upper punch was lowered during compression while the lower punch was kept stationary. A mixture of spherical sugar particles and glass ballotini ($n < 100$, as marker particles) was loaded into the rig. The powder mixture was compacted in discrete steps outside the XμCT setup using a universal testing machine. After each compression step, the position of the upper punch was fixed and the rig was transferred into the XμCT instrument for image acquisition. Fu et al. used their watershed algorithm to locate the glass ballotini in the powder bed and trace their position between the different compaction steps (Fig. 4). Even though the tracer particles exhibit different mechanical and surface friction forces compared to the sugar spheres, it was assumed that they followed the local motion of the surrounding material. The results of the compaction experiments were promising. By quantitative analysis of the tracer particle positions with increasing compression force the authors were able to detect wall friction effects at the die-wall boundary (Fig. 4B).

Traini et al. used XμCT to qualitatively study drug release from a modified drug release tablet [29]. In this osmotic release oral system (OROS), the tablet is coated on the outside with a semi-permeable membrane and divided internally into two compartments separated by a further impermeable membrane. One of the compartments contains a polymer matrix, while the other compartment contains the drug formulation. Driven by the osmotic pressure, the polymer matrix swells upon water uptake and actively pushes the contents of the drug containing second compartment through a small hole in the tablet coating. This system can be used for zero order drug release products. In their study, Trani et al. imaged tablets before dissolution and at 14 and 24 h during dissolution. The samples from the dissolution study were dried at 50 °C for one hour before characterisation by XμCT (Fig. 5). It was possible to distinguish the two compartments of the tablet before disso-

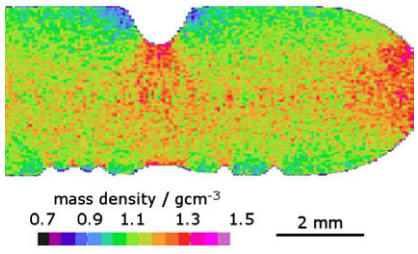

Fig. 2. Density distribution within a direct compressed MCC tablet over a cross-section through the *yz* plane. In this projection the tablet is embossed on the bottom surface and exhibits a break-line on the top surface (Reprinted with modifications from [25] with permission from Elsevier).

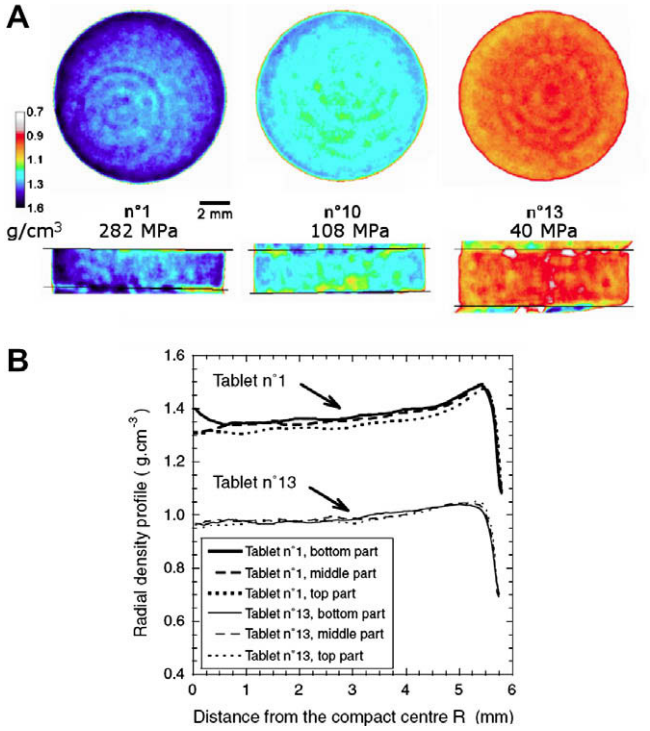

Fig. 3. (A) False-colour maps of the quantitative density distribution in three different model tablets. The top row shows the *xy* plane at mid-height; the bottom row shows the *yz* plane. (B) Radial density profiles for the cross-sections in *xy* plane at mid-height of the compacts (Reprinted with modifications from [26] with permission from Elsevier).

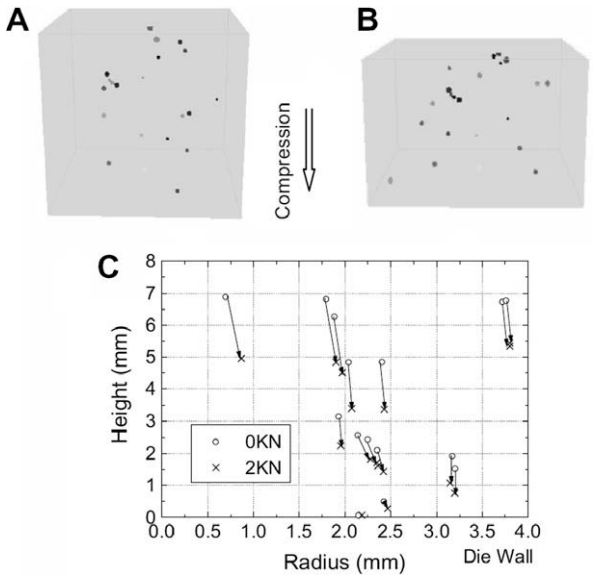

Fig. 4. (A and B) 3D maps showing the position of tracer particles in a powder bed before (A) and after (B) compression at 2 kN. (C) Respective displacements of the marker particles in radius-height coordinate system. Wall friction effects can be observed for tracer particles located near the die wall as their displacement is shorter compared with the particle displacement at the die centre. The displacement of the tracer particles decreases towards the lower (stationary) punch (Reprinted with modifications from [27]. Copyright Wiley-VCH Verlag GmbH & Co. KGaA. Reproduced with permission).

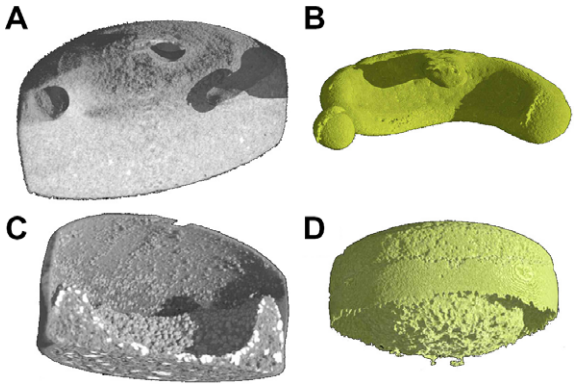

Fig. 5. Reconstructed 3D models of a OROS controlled release dosage form after 14 h (A and B) and 24 h (C and D) of dissolution testing. Voxel size $8 \cdot 8 \cdot 8\ \mu m^3$ (A and C) show the overall morphology of a virtual cross-section through the dosage form. (A) The membrane between the two compartments cannot be resolved, yet the different phases can be discerned: the drug containing phase in the upper part of the image exhibits a slightly stronger X-ray attenuation. (B) Model of the void space in (A) of the released, previously drug containing, phase after 14 h. (C) After 24 h the entire drug containing phase is released. (D) Corresponding void space in the remaining tablet shell (Reprinted with modifications from [29]. Copyright Wiley-VCH Verlag GmbH & Co. KGaA. Reproduced with permission).

lution as well as after 14 h into the dissolution process. No membrane between the two compartments was reported. Based on the reconstructed cross-sections, the authors modelled the void space that was observed in the tablet shell after drying the samples from the dissolution experiments. However, the void space observed in the tablet in these experiments is not representative of the structure of the tablet during dissolution. It is very likely that the morphology of the internal tablet structure has changed over the drying period. No quantitative data recording the evolution of observed void volume over dissolution time were presented.

The first example of *in situ* imaging of a pharmaceutical dosage form during dissolution by XμCT was reported in a paper by Karakosta et al. [30]. Model tablets of diltiazem hydrochloride and Eudragit RSPO (3 mm in diameter) were compressed and imaged over a total of 5 h while exposed to distilled water. The acquisition of each sample took 40 min, and the resulting image resolution was $10 \cdot 10 \cdot 10\ \mu m^3$. The results obtained by XμCT, which is sensitive to the electron density distribution in the sample, were compared to the results of the same experiments performed by ^1H MRI (see the next section), in which the signal was dominated by hydrogen species with sufficiently long relaxation time for imaging experiments. Even though the contrast between the water and the polymer matrix in the XμCT images was found to be rather poor, the technique was found to be well suited to study the evolution of air voids within the tablet matrix during water ingress (Fig. 6A–H). Using the image data for the different time points during dissolution it was possible to quantify the air-void size distribution in the whole tablet volume (Fig. 6I). The results of the air-void evolution were discussed in terms of two diffusion coarsening models: Ostwald ripening and diffusion of droplets into contact followed by coalescence. Based on the distribution function of the air voids and the fact that sudden collapse of some voids was observed experimentally, it was concluded that the coalescence model describes the observations best. The authors suggested that the air voids might play a role in the initial wetting of the porous medium and its structural integrity.

Chauve et al. analysed the changes in morphology upon dissolution of small pellets made of high-amylose starch by XμCT and

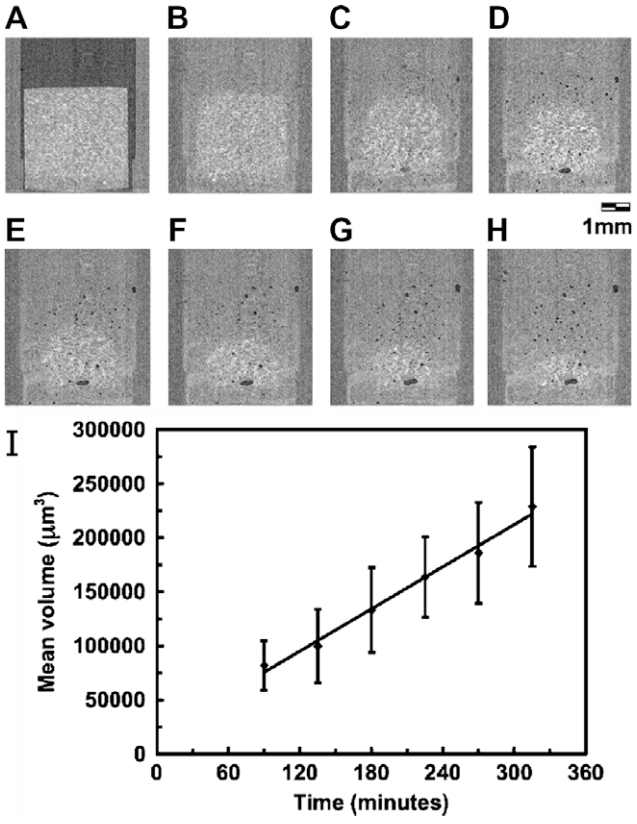

Fig. 6. The central coronal slice extracted from a three-dimensional XμCT data set. Slice (A) is the dry matrix. Air appears dark and the side grey stripes are part of the polymer tube supporting the sample. Slices (B–H) show the same slice exposed to water for the following times: 45, 90, 135, 180, 225, 270, and 315 min. Water appears as light grey, comparable to the tablet. (I) The increase in the mean air-void volume in μm^3 with respect to time. (Reprinted with modifications from [30] with permission from the American Physical Society).

electron microscopy [31]. The pellets, which were prepared by compacting spray-dried powder of the excipient, were imaged in the dry state and after they were exposed to distilled water for different amounts of time. For the XμCT experiments, the pellets which had been in contact with water were either imaged directly or freeze-dried prior to the acquisition, while all pellets analysed by electron microscopy were freeze-dried. In both the XμCT cross-sections as well as the scanning electron images, which were acquired after cutting through the pellets with a razor blade, a membrane between a porous outer layer and the core of the pellet was observed. This membrane could not be distinguished from the hydrating water in the XμCT experiments using wet pellets, as the contrast between the membrane and the water was insufficient. The authors assume that the freeze-drying process preserves the real texture in the pellets by preventing a collapse of the structure and does not lead to artefacts itself. It is concluded that upon dissolution water initially quenches the pellet surface and then continues to penetrate the core. In the second step, the membrane formed during the quenching develops into a hydrogel and the water movement becomes diffusion controlled. Similar samples were also analysed by MRI (see the next section).

Among other techniques, XμCT was used by Inman et al. to characterise fracture in bilayered MCC tablets [32]. Wedges of fractured bilayer structures were analysed, and it was possible to localise cracks in the tablet matrix. Based on the results from XμCT, the authors concluded that the stress relaxation during the two-stage compression of bilayered tablets occurs most likely in the radial direction immediately after ejection of the tablets from the die.

3. Magnetic resonance imaging (MRI)

As outlined in the last section, the contrast in XμCT is achieved by the attenuation of photons as a result of absorption, refraction or scattering when a collimated beam of X-rays is used to illuminate the sample specimen. As a consequence of their photon energy, it is through the interaction with the electrons of the sample material that X-rays are attenuated. In contrast, in nuclear magnetic resonance (NMR) the magnetic moments of certain nuclei in the sample, which is placed in an external magnetic field B_0, align with this field, and then can be excited with a pulse of radiation. The excitation of the nuclei leads to the absorption of photons and subsequent re-emission, which is measured as the NMR signal. A short introduction to nuclear magnetic resonance in the context of this review is provided in Section 1.2.1, which is available in the online supplementary material.

3.1. Tomographic imaging principles

The concept of generating a spatially resolved NMR signal for tomographic experiments was first demonstrated by Lauterbur by imaging two test tubes of water surrounded by D_2O [33]. At the same time, Mansfield and Grannell published their findings of NMR 'diffraction' in solids which made use of the same concept [34]. Lauterbur referred to this technique as *zeugmatography* but despite the impact of his paper, he was awarded the Nobel Prize for this work in 2003 together with Sir Peter Mansfield, this term did not prevail. In magnetic resonance imaging (MRI), as the technique is now commonly referred to, spatial resolution is introduced to the NMR experiment by applying one or multiple magnetic field gradients G in addition to B_0.

$$\omega_y = \gamma(B_0 + G_y y). \quad (1)$$

Here, G_y refers to a gradient in the y direction (γ is the gyromagnetic ratio and ω is the frequency as detailed in Section 1.2.1 of the online supplementary material). The additional gradient has the effect of slightly shifting the resonance frequency of the sample nuclei within the magnetic field depending on their position (Fig. 7). The resonant frequency ω becomes a function of the sample position in real-space and by applying gradients in the x, y and z directions three dimensional tomographic images can be acquired. Further details on the background of MRI are beyond the scope of this review, and the reader is referred to the literature introducing MRI in a chemical engineering context [35,36] and more detailed textbooks on the technique itself [37,38].

MRI images of solids are typically acquired indirectly by measuring the signal of liquids interacting with the dosage form rather than imaging the solid phase directly. On standard imaging setups, it is not possible to readily acquire images with sufficient spatial resolution from solid materials. This is due to line broadening and extremely short T_2 times in solids, which leads to a very low NMR signal. However, new imaging sequences, such as SPRITE [39], have been successfully applied to image rigid polymers, and it is quite possible that along with future developments in MRI technology, MR imaging of solids will become more attractive in the future.

3.2. Pulse sequences

In order to acquire the information that is required to reconstruct MR images, a number of different so-called pulse sequences are used. The pulse sequence describes the timing, strength and sequence of the r.f. pulses and gradient pulses that are applied, and usually repeated for a large number of cycles, for the MRI experiment. The pulse sequence is usually described in an abstract schematic as it needs to be adapted to the specific conditions of different magnets, coils, amplifiers and software on each MRI instrument.

A large number of pulse sequences have been developed, which allow MR images to be acquired under a variety of conditions and acquisition speeds and which also allow us to measure a number of different properties, such as the spatial distribution of velocity of flowing liquids in a sample. The pulse sequences also enable the operator to enhance the contrast within MR images depending on the physico-chemical properties of the samples, e.g. the T_1 or T_2. The sequences are distinguished by a tremendous number of acronyms such as RARE, GERVAIS or SPRITE, and whole books have been dedicated to the topic [40]. Most often basic pulse sequences such as the spin-echo sequence have been used for pharmaceutical MRI applications to date, and the reader is referred to the literature for further details of specific pulse sequences [41].

So far, MRI has been widely applied for quantitative analysis of chemical products and processes [42] and in chemical processes and reaction engineering [43]. Melia et al. and Richardson et al. provided first overviews of different applications for MRI to characterise controlled release pharmaceutical dosage forms [44,45].

3.3. Pharmaceutical applications

The majority of the research activities in the field of imaging pharmaceutical dosage forms with MR techniques have focused on studying the hydration of polymers of matrix tablets. Only a few groups have studied pellets or other dosage forms and only one study on film-coated tablets has been reported so far. Typically, a flat faced tablet with a diameter of less than 1 cm and a thickness of several millimetres is used as a model tablet system, and a standard spin-echo imaging sequence is employed for the image acquisition. Table S.1 in the electronic supplementary materials of this article gives the full details of the work published to date [30,46–78]. Due to the amount of work in the field and the restriction in space, we will only highlight some selected studies in more detail in this section.

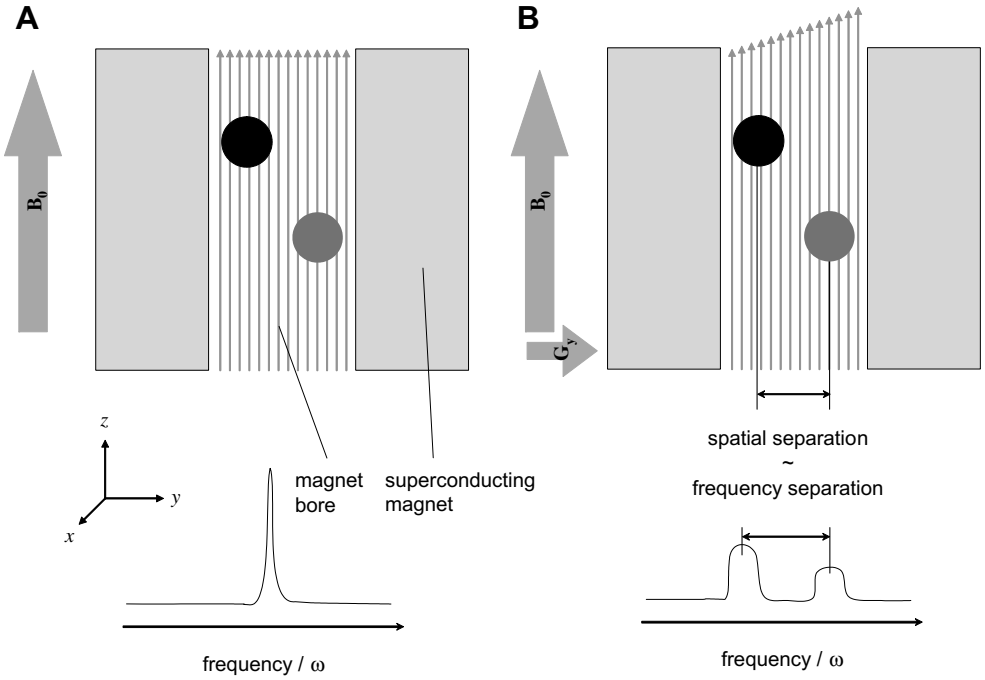

Fig. 7. Principle of an MRI experiment. (A) Normal NMR experiment. The resonance frequency ω_0 is determined by the static magnetic field B_0 and the gyromagnetic ratio γ. All nuclei in the magnetic field resonate at the same frequency. (B) By applying a gradient of an additional magnetic field G_y, the observed resonance frequency becomes a function of the position of the nuclei in real space. The vector arrows in the magnet bore indicate the magnetic field in the magnet (Reprinted with modifications from [35] with permission from Elsevier).

The first application of MRI to study pharmaceutical tablets was published by Nebgen et al. [46,79]. By immersing tablets in silicon oil spiked with a gadolinium complex, it was possible to image the three-dimensional void space, filled by the oil, within the tablets. Three different types of tablets were analysed: placebo tablets made of MCC, drug-loaded MCC tablets and compression-coated tablets. The spatial distribution of porosity as a function of the compression used for the compaction of the MCC tablets was analysed and compared to the bulk porosity as determined by gas pycnometry. In the compression-coated tablets it was possible to detect hairline cracks running from the core through the entire erosion matrix coat to the tablet side faces.

Rajabi-Siahboomi et al. studied the formation and growth of a hydrate pseudogel layer on the surface of flat faced hydroxypropylmethylcellulose (HPMC) tablets as a function of immersion time in water [47]. The tablets were fixed onto a sample mount during the immersion and imaging experiments and the water was removed prior to the image acquisition. Uniform growth of the gel layer was observed in the radial and axial planes of the tablet. The dimensions of the tablet core exhibited an anisotropic change: while the tablet core shrank in the radial plane of the tablet, expansion was observed in the axial plane. This behaviour was tentatively assigned to a release in compression stress along the axial direction of the tablet as a result of water uptake. The edges of the tablets were found to hydrate to a greater extent than at the centre of the tablet faces.

While all the previous MR imaging work on pharmaceutical dosage forms was qualitative, Hyde et al. published the first quantitative study investigating the ingress of water in PBS buffer into monolithic implants made of poly(glycolic acid-co-DL-lactic acid) (PGLA) produced by an extrusion process (Fig. 8) [51]. The results of the spatially resolved MRI method were compared to the gravimetric determination of water uptake, and excellent agreement was found between the two techniques. Depending on whether API was loaded into the polymer matrix or pure polymer (placebo) was exposed to the buffer solution, the kinetics of the PBS ingress was very different. While the unloaded PGLA matrix was saturated with PBS after 80 min, the process took more than 74 h in the presence of goserelin, a large peptide molecule used as the model API for this study. This effect was attributed to the changes in the physical structure of the polymer introduced by the API molecule. Along with this strong increase in penetration time, a change in the transport mechanism was detected by the quantitative analysis of the MR images.

The erosion of a soluble API containing tablet core embedded in a much more slowly disintegrating polymer matrix by dry coating was the subject of a study by Fahie et al. [54]. MRI was used to elucidate the mechanism of erosion of the API containing compartment in two different formulations of the controlled release tablets. The formulations were different in composition and processing of the outer 'scaffolding shell', which covered the top and bottom surfaces of the tablet but not the central band (see Fig. 10 for a similar system). A strong dependency of the drug release profile on formulation was observed by dissolution testing. The MRI experiments revealed distinct qualitative differences in the porosity of the release rate controlling coating barrier on the top and the bottom of the tablet. The formulation that exhibited higher porosity of these areas correlated with faster release of the drug. Based on the MRI images, the authors were able to dismiss an alternative mechanism of accelerated drug release that had been suggested based on destructive visual inspection of samples during dissolution testing. All experiments in this study were performed under static dissolution conditions.

Narasimham et al. investigated the distribution of molecular mobility during dissolution in poly(vinyl alcohol) (PVA) tablets [59]. The ingress of water into model tablets was imaged by one-dimensional imaging of the water distribution and the self-diffusion coefficient of the water molecules in the polymer. Depending on the molecular weight of the PVA and the location within the tablet, differences were found in the kinetics of the hydration

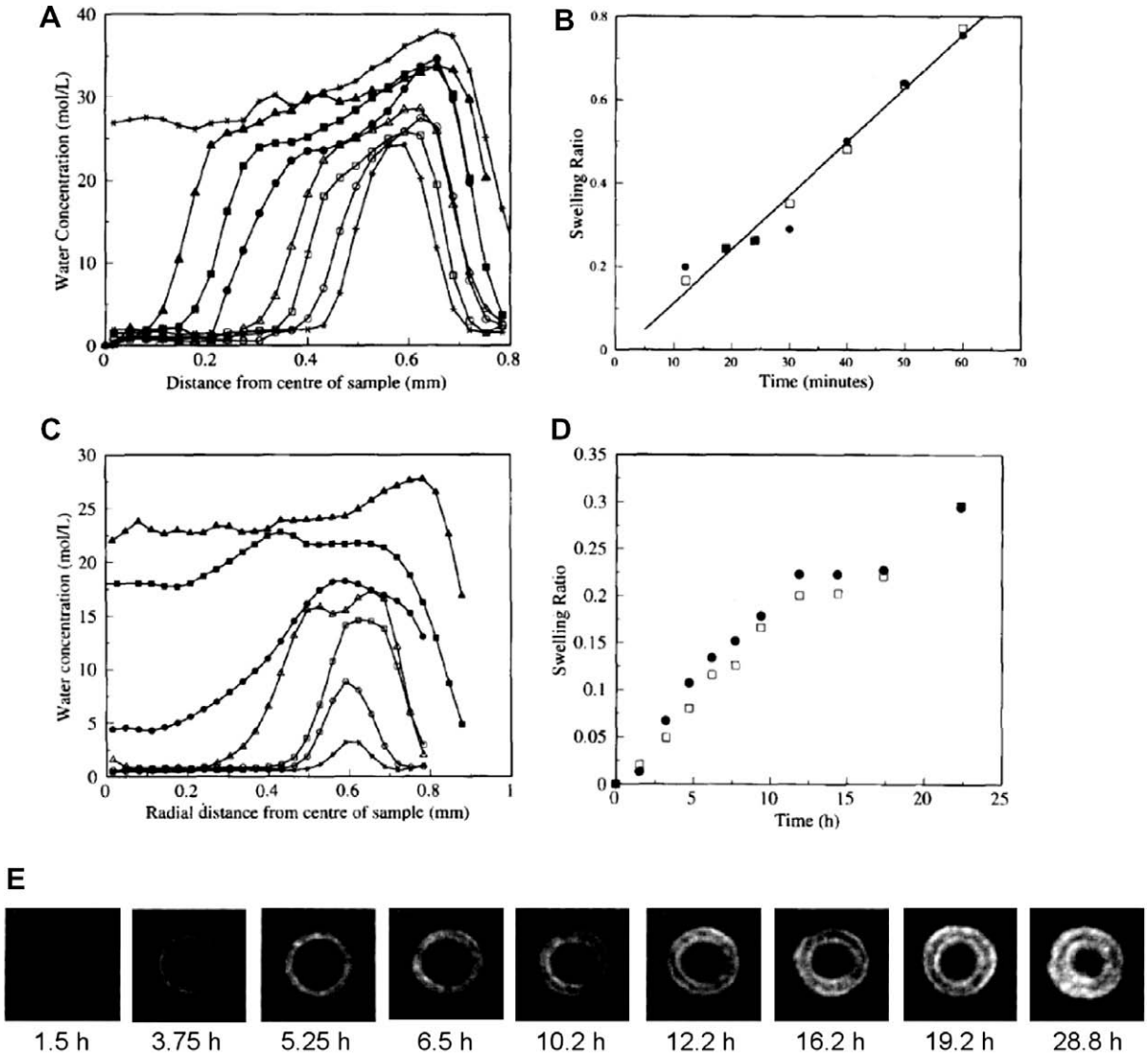

Fig. 8. Quantitative MR imaging of the buffer uptake in a monolithic implant of poly(glycolic acid-co-DL-lactic acid) (PGLA) unloaded (A and B) and loaded with API (C–E). (A) Radially averaged water concentration profiles acquired during the penetration of PBS buffer into the placebo implant between 12 and 80 min. (B) Weight uptake of PBS in the placebo samples (gravimetic data • and NMR data □). (C) Radially averaged water concentration profiles of the drug loaded PGLA implant between 1.5 and 234.3 h. (D) Corresponding weight uptake of PBS (gravimetic data • and NMR data □). (E) Images of the PBS ingress into the drug-loaded implants (Reprinted with modifications from [51] with permission from Elsevier).

and the diffusion mechanism (Fig. 9). The experimental results were compared to the predictions based on a mathematical model of polymer dissolution. Good consistency between the experimental results and the theoretical predictions was found.

The first example of an *in situ* imaging study of tablet dissolution under non-static conditions was performed by Fyfe et al. [61]. For the imaging experiment, a modification of a commercial flow through cell (USP apparatus IV) was developed that could be fitted within the diameter of an MR imaging coil. Three different controlled release dosage forms were investigated with this setup: a HPMC placebo tablet, a dry-coated tablet and an osmotic pump tablet similar to the one investigated by Traini et al. [29]. The imaging experiments were performed under both static and flow conditions with flow rates up to 16 ml min^{-1}, and the images were purely qualitative. While fast flow rates can lead to distortions and artefacts in the images, the authors found that the flow rates used for their experiments were too low to cause such effects. Differences in HPMC dissolution were found upon comparison of the images acquired under static and flow conditions. Mechanical shear at the surface of the dissolving HPMC caused decreasing thickness of the gel layer as the flow rate increased. These experiments highlight the importance of performing the MRI experiments under the same conditions as those used in traditional dissolution testing, if the results are to be compared.

Sutch et al. used MRI for the investigation of pulsatile release capsules [68]. Pulsatile release capsules consist of a capsule body, which is coated with a water insoluble polymer, and a release controlling plug that seals the capsule and erodes with time. Once the dissolution medium penetrates the capsule it contacts an excipient that leads to expulsion of the API content upon hydration. In this study, the performance of capsules that were coated using either aqueous or organic coating processes was analysed. The capsules with the aqueous coating were found to exhibit premature and erratic drug release. Coating formulations based on organic solvents showed the desired pulsatile release profile. Based on the MR images, it was proposed that the early release of the capsules based on the aqueous coating formulation was caused by the poor seal between capsule and plug of this capsule and subsequent prema-

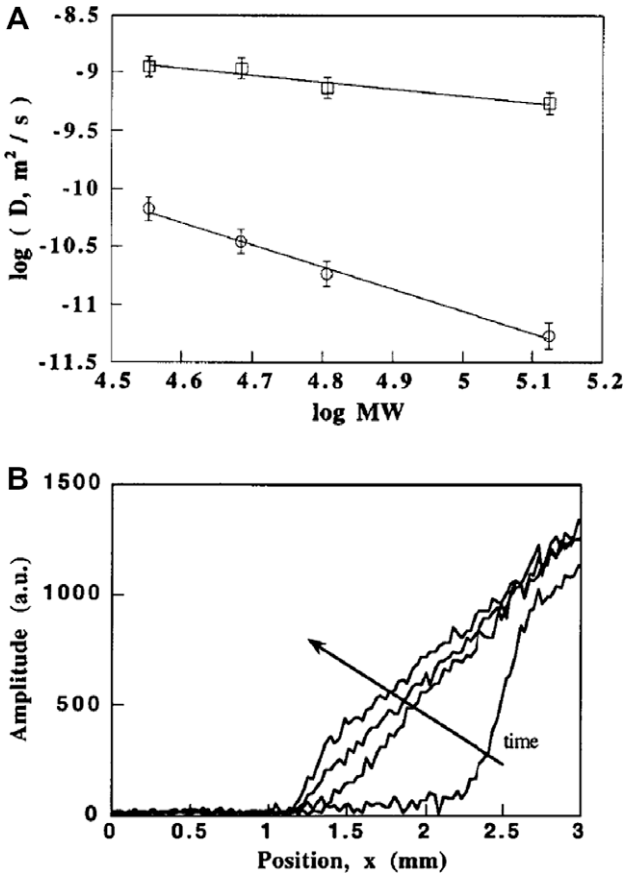

Fig. 9. (A) Log–log plot of the molecular self-diffusion coefficient in PVA tablets after 30 min hydration extracted from one-dimensional MR images. The self-diffusion changes between the different interfaces of the tablet: the slope at the interface between the hydrated PVA and the inert substrate (circles) is −1.9, which agrees with predictions for repetition-diffusion, while it is −0.6 at the interface between PVA and the water (squares), indicating Zimm type diffusion. (B) One-dimensional water concentration profiles acquired after 2 min, 30 min, 1 h and 2 h for a sample of PVA with a molecular weight of 133,000. The interface with the inert substrate is located at $x = 1$ (Reprinted with modifications from [59], Copyright 1999 American Chemical Society).

ture hydration of the expulsion agent. For the studies, a combination of two-dimensional spin-echo images and images acquired with the RARE sequence was used.

Djemai and Sinka have quantified density variations in tablets [72]. In an approach similar to Nebgen et al. [46], tablets were immersed with mineral oil under vacuum. A saturation of 95% of the pore space by the oil was estimated. A set of flat faced cylindrical MCC tablets of uniform density was prepared, and their density was determined by their weight and dimensions. This set of tablets was used as a calibration set such that the MRI signal from the pore space of the tablet could provide a measure of tablet density (Fig. 11). Different sets of production tablets were analysed using the MRI method and the density distribution within the dosage form was determined. The results of the MRI experiment were compared to a previous study on the density distribution in tablets measured by XμCT by Sinka et al. [25] and good agreement was found between the two techniques.

4. Terahertz imaging

4.1. Measurement principles

Terahertz radiation has an excellent potential in the advancement of our understanding of pharmaceutical solid dosage forms

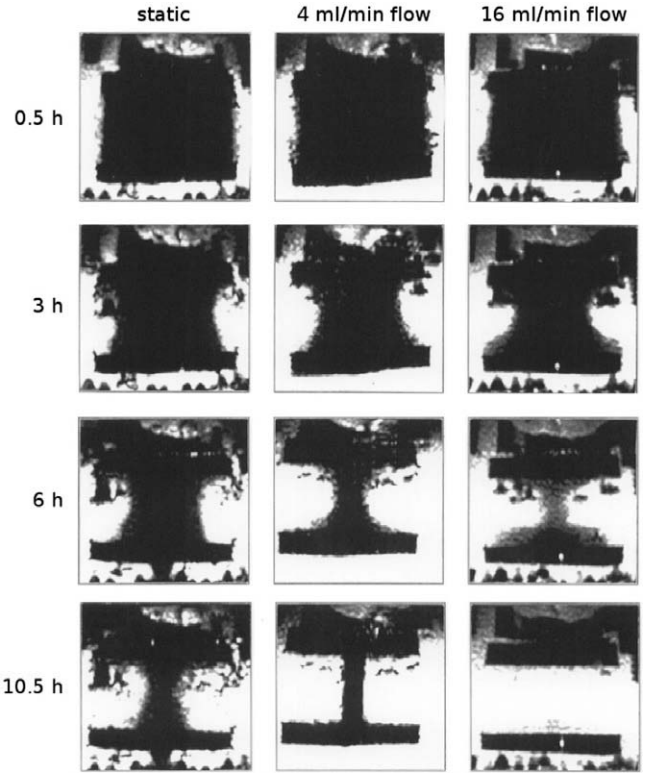

Fig. 10. MR images acquired *in situ* during dissolution of a dry coated controlled release tablet using a modified USP flow through cell at different flow rates (Reprinted with modifications from [62] with permission from Elsevier).

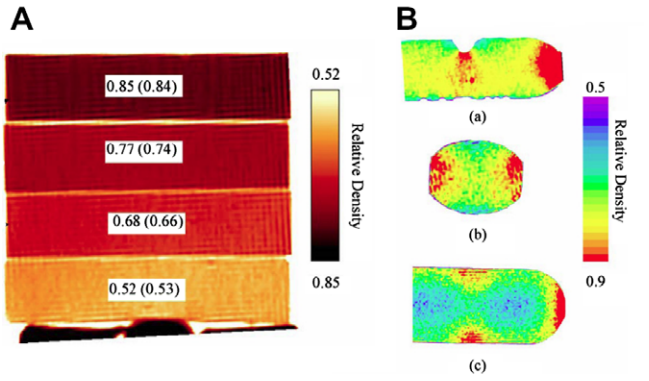

Fig. 11. Quantitative imaging of tablet density by MRI (A) Calibration of the MRI technique using a stack of flat faced model tablets of MCC compressed with 1–4.9 kN. Values in brackets refer to the theoretical relative density from weight and dimension measurements. (B) Relative density maps of cross-sections through the three principal axis in a tablet. All densities are stated in g cm^3 (compare (A) to the results from XμCT in Fig. 2, (Reprinted with modifications from [72] with permission from Elsevier).

but is, as yet, under-explored. The recent developments in semiconductor physics and ultrafast laser technology have made it possible to provide light at terahertz frequencies (a frequency of 1 THz equals a wavelength of 0.3 mm) in a relatively simple way [80,81]. Light located in this range of the electromagnetic spectrum, at energies between the infrared and microwave region, was very difficult to generate previously [82]. It has unique properties in that it easily penetrates through most plastics and polymeric materials used as excipients for pharmaceutical tablets and, at the same time, it reveals a wealth of information about the medium and long range interaction of small organic molecular crystals, which are the typical active ingredients of most modern medicines.

The breakthrough for the generation and detection of coherent terahertz radiation only dates back to as far as the late 1980s when researchers at the Bell labs developed the photoconductive antenna technology on which modern terahertz emitters and detectors are based [81]. This technology combines approaches from both optics and electronics in order to bridge the gap of the electromagnetic spectrum, where only very weak sources and detectors were available previously.

The emitter and receiver devices used to generate and detect terahertz radiation are made of GaAs, a III–V semiconducting material, with a band gap of 1.42 eV. Pulses of terahertz radiation are generated, when charges are accelerated across this material. In order for this to happen, two electrodes with a gap in between are patterned onto a flat wafer of the semiconductor. A DC electric field is then applied between the two electrodes. As the electrodes are connected through a semiconductor, no charges can move between the electrodes, a configuration comparable to an open switch. This setup is called a biased photoconductive antenna. The photoconduction occurs when a short pulse of light with a photon energy $h\nu$ (h Planck constant and ν frequency) exceeding the band gap of GaAs, that corresponds to a wavelength of less than 873 nm, is directed onto the gap between the electrodes. Electrons and holes form on the surface of the device as the electrons in the semiconductor are excited from their valence band into the conducting band. Due to the DC bias voltage between the electrodes, the photo-injected charges are then accelerated towards the electrodes, and as a result of the charge acceleration an electric field is emitted – the terahertz pulse.

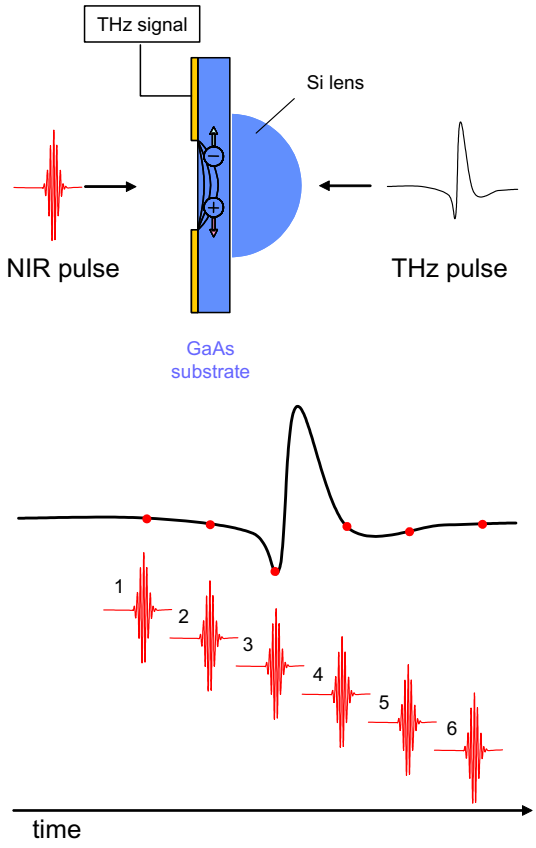

Fig. 12. Principle of coherent photoconductive detection of the terahertz electric field in time-domain terahertz spectrometers using a low-temperature grown GaAs antenna. Using a delay line the NIR gating pulse is systematically delayed with respect to the terahertz pulse (simplified as measurements 1–6 in this illustration) and the electric field of the terahertz pulse is measured in consecutive measurements.

The detection of the terahertz pulse is achieved through the reverse process (Fig. 12). Rather than applying a bias voltage across the semiconductor, during detection the sub-picosecond terahertz pulse is focused onto the device using a hemispherical lens with a similar refractive index to the GaAs. Simultaneously, a femtosecond pulse of NIR light is focused onto the gap between the electrodes on the opposite face of the semiconductor. The NIR pulse, which is derived from the same NIR laser beam used to generate the terahertz pulse, is called the probe pulse and is used to optically gate the semiconductor switch by generating charge carriers in the device. These charge carriers are then accelerated by the terahertz pulse. The resultant photo-induced current, which is proportional to the terahertz electric field, is measured between the electrodes. By sweeping the delay of the NIR pulse relative to the terahertz pulse, the electric field of the pulse can be sampled. The repetition rate of the pulses is typically around 80 MHz, and with fast optical delay lines and fast data acquisition interfaces the whole terahertz waveform can be acquired within milliseconds. Using this coherent detection scheme, no cryogenic cooling is required to distinguish the terahertz radiation from the thermal background.

The development of terahertz technology was facilitated by substantial advances in laser technology over the last decade leading to a reduction in size, cost and availability of femtosecond lasers. Typically, titanium sapphire lasers operating at 800 nm central wavelength with a pulse duration between 10 and 100 fs are used for the generation and detection of terahertz radiation.

Terahertz time-domain spectroscopy (THz-TDS, often also referred to as terahertz pulsed spectroscopy, TPS) is an ideal probe for the physical characterisation of pharmaceutical solids [83,84]. It is non-destructive, and interacts with vibrational modes that extend across large domains of the lattice in organic molecular crystals [85]. The ability to probe the lattice dynamics which represent interactions between molecules in their crystal structure makes terahertz spectroscopy a very powerful tool for the analysis of complex solid-state materials properties [86,87]. In terms of imaging applications of terahertz radiation, a detailed overview of different techniques and applications has been published recently by Chan et al. [88].

4.2. Time-resolved terahertz pulsed reflection imaging

In addition to tomographic imaging using reconstruction algorithms, it is also possible to explore the structure of a pharmaceutical dosage form using time-resolved analysis of the back reflections of a pulse of radiation that is able to penetrate the dosage form. To date, this imaging technique, called terahertz pulsed imaging (TPI), is the most commonly used terahertz imaging approach for the characterisation of pharmaceutical solid dosage forms.

In TPI terahertz light can be used to probe the internal structure of a solid dosage form [89]. Most of the excipients that make up the bulk of a tablet are transparent to terahertz light, whereas the drug and interfaces from different coating layers or substructures within the tablet lead to a contrast in the images due to a change in their refractive index. When ultra-short pulses of coherent terahertz radiation are directed onto the surface of a coated tablet, part of the pulse is reflected from the surface of the coating while the remaining photons are propagating into the coating (Fig. 13). With an average power of the terahertz radiation in the μW range, there is no thermal stress induced in the sample. The concept of structural imaging is based on the experiment by Mittleman et al. [90] and was subsequently applied to image pharmaceutical dosage forms by Fitzgerald et al. in 2005 using the example of a sugar-coated tablet [91].

The ratio of the reflected to the transmitted radiation is given by the dielectric properties of the coating material. As the terahertz

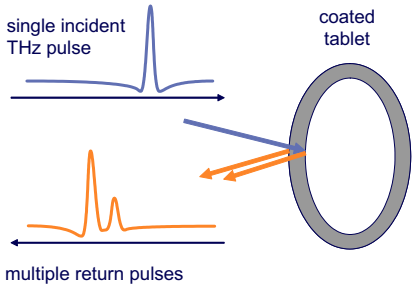

Fig. 13. Principle of non-destructive time-of-flight structural imaging of a coated tablet using ultra-short pulses of coherent terahertz radiation. A pulse of coherent terahertz radiation is reflected at each interface with a change in refractive index as it propagates into the tablet.

pulse propagates deeper into the dosage form further reflections occur whenever there is a change in real refractive index, such as at the interfaces of coating layers. Time-resolved detection of the reflected pulses is performed to record the time-domain waveform of the reflected terahertz pulse (Figs. S.3 and S.4 in the online supplementary material). The thickness of all coating layers that the pulse has propagated through can be determined non-destructively using the time-of-flight between the pulses and the refractive index of the coating material.

A single terahertz time-domain waveform, which contains the information characterising the coating structure at one specific point on the surface of the dosage form, can be acquired in about 50 ms. In order to examine the whole solid dosage form in detail, it is necessary to acquire the terahertz waveforms over the surface of the tablet. For the measurement of the waveform at each spot, the tablet has to be presented to the terahertz optics at an angle of normal incidence. Fortunately, this task can be achieved conveniently by using an automated terahertz tablet scanner. As a first step, the instrument generates a model of the three-dimensional surface dimensions of the entire tablet (Fig. S.5 in the online supplementary material). The tablet is held by a robot arm that is able to present any point on the surface of the tablet at an angle of normal incidence to the terahertz optics. The surface model is stored and can be used as the basis for the subsequent terahertz mapping. For the imaging of multiple tablets of identical geometry the same surface map can be used, thus reducing the acquisition time by a factor of two.

By mapping over the entire surface of the tablet, the statistical distribution of the coating thickness and its quality can be quantified (Fig. 14). Even though the lateral spatial resolution of terahertz images in the *x* and *y* directions is diffraction limited to about 50–200 μm due to the long wavelength of terahertz radiation, the axial resolution in *z* direction, a function of the pulse duration, is better than 40 μm [89].

The first example of how TPI can be used to study film-coated tablets was demonstrated by Zeitler et al. [89]. In this study, the potential of the technique to characterise a wide range of commercially available pharmaceutical dosage forms such as film-coated tablets, layered tablets and soft gelatine capsules was investigated. In the same study, the TPI instrument that is capable of performing the fully automated terahertz mapping experiment of all surfaces of a dosage form was introduced. Depending on the overall surface area of the dosage form an acquisition time between 20 and 50 min was required for modelling the surface and recording a three-dimensional terahertz map of a film-coated tablet.

In application to sustained-release tablets, TPI was further evaluated for pharmaceutical applications by Ho et al. [92]. The thickness measurements obtained non-destructively by TPI were validated against measurements of cross-sections through the

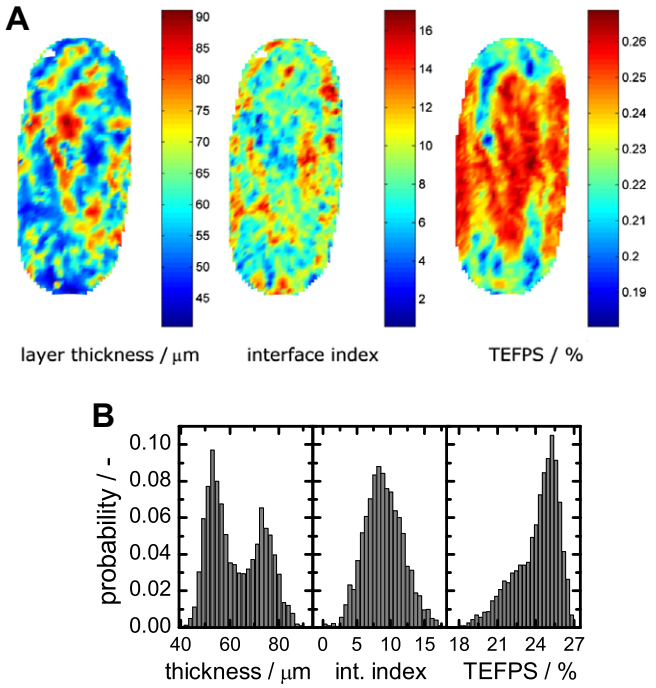

Fig. 14. (A) Colour coded maps showing the spatial distribution of coating thickness, interface index (the ratio between the reflection from the surface and the coat/core interface) and the terahertz electric field pulse strength (TEFPS) over the surface of the tablet. (B) Statistical information of the coating thickness and quality parameters over the surface of the tablet face.

same sample specimens by optical microscopy. Very good agreement was found between the two techniques. While the microscopy technique provided a very limited number of data points over the surface of the sample, and the technique is inherently destructive, TPI was found to provide much greater statistical usefulness as the number of sample points over the surface of the tablet was higher by several orders of magnitude than that associated with optical microscopy. The ability to detect and quantify the extent of coating defects by TPI further highlighted the rich information content provided by terahertz structural images to assess the reproducibility, uniformity and distribution of film coating layers. Important insights to aid process development have been obtained. For example, in development of film coating technology, weight gain data during coating are used and it is assumed that a uniform distribution of the film exists over the whole surface of the tablet.

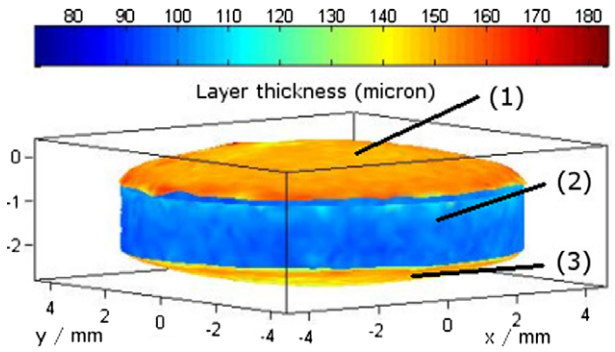

Fig. 15. Three-dimensional model of the coating thickness distribution over the surface of a tablet. The coating thickness at the central band (2) is significantly lower compared to that on the faces of the tablet (1) and (3) (Reprinted with modifications from [92] with permission from Elsevier).

Ho et al. demonstrated that this is not always an appropriate assumption (Fig. 15).

In a study by Spencer et al., the coating thickness as measured by TPI of three different enteric coated tablets was correlated with the mean dissolution time (MDT) of the respective tablets [93]. The results of the film thickness measurements revealed that the mean coating thickness varied between 57 and 109 μm between the different tablets. The inhomogeneity in thickness is surprising given that the tablets used for this study were marketed products that had been sourced commercially. As the TPI experiments are non-destructive, it was possible to perform dissolution testing on the same samples that were used for the coating thickness determination. A modest correlation was found between mean coating thickness and MDT. However, it was acknowledged that the delayed-release system was more complex and coating thickness was only one factor contributing to the dissolution performance amongst others. The authors speculated that the exposure of the tablets to media of different pH under different shear stress conditions as required by the modified USP procedure for dissolution testing of delayed-release tablets (50 rpm stirring in 500 ml at pH 1.2 for 2 h; followed by 100 rpm stirring in 900 ml at pH 6.0 for 1 h; followed by 50 rpm stirring in 900 ml at pH in the range between 6.5 and 7.2 until dissolution) will have an impact on the dissolution behaviour beyond the factors that are solely affected by the coating thickness, and further work is required to understand this process in more detail.

For the case of sustained-release tablets produced under lab and pilot scale conditions, Ho et al. further investigated the applicability of TPI to correlate coating parameters obtained by TPI with the dissolution performance of the dosage form [94]. Even though the tablets from lab and pilot scale batches were coated to the same weight gain, the MDT was found to be significantly longer for the pilot scale tablets. TPI was able to discriminate the two batches based on significant differences in the coating thickness even though the weight gain was identical. In addition to the coating thickness, the authors highlighted that changes in coating density, which can be extracted from the relative reflectivity of the coating compared to a reference mirror, form a very important parameter that can be used to assess the quality of film coatings by TPI. The correlation between coating thickness and MDT was very clear and much stronger than in the study by Spencer et al.

The effect of material density on the refractive index of a tablet has been demonstrated previously by Pore et al. [95]. For example, for two different filler excipients an increasing refractive index was found with increasing tablet hardness due to changes in compaction force and speed. It was possible to detect concealed cracks in tablets by TPI and the results were validated by XμCT. While the combined acquisition and data processing time in TPI was about 30–45 min the process took several hours in XμCT with the same samples. By combining the data acquired with TPI on a set of model tablets of different density with a partial least squares calibration, Palermo et al. were able to map density differences on the surface of tablets [96]. The increase in refractive index with increasing compaction force which was reported in the study by Palermo et al., based on the tablets made from a mixture of four excipients, agree with the findings of Pore et al., which are based on single component compacts.

Ho et al. evaluated the applicability of TPI for understanding of process scale-up [97, in this issue]. One-hundred and ninety sustained-release tablets were sampled during the scale-up operation of a film coating process from the lab to the pilot scale and analysed by TPI. Dissolution testing was performed on the same tablets, and the results from TPI analysis and dissolution testing were correlated. In terms of the amount of polymer applied, the traditional parameter that is used for process control and to assess the coating quality, no significant differences between the lab and pilot scale were found. However, the MDT of the pilot scale batch was twice as long compared to the lab scale batch. It was found that within a batch, variations in film layer thickness were most strongly correlated to the MDT. The significant difference in MDT between lab and pilot scale correlated to the differences in film density as measured by TPI. The results of this study not only suggest that TPI can be used for the non-destructive evaluation of the film thickness, but also that the information obtained from the imaging experiment contains much more quantitative information on the physico-chemical properties of the coating that can be used to assess its quality.

Shen et al. showed examples of how the reflected terahertz pulses can be used not only to study the structure of a dosage form, but also investigate its chemical composition [98]. Using the reflection from a mirror as a reference, the absorption coefficient α and refractive index n can be extracted from the sample reflection

$$n(\nu) + i\frac{\alpha(\nu)}{4\pi\nu} = \frac{1 - P_s(\nu)/P_m(\nu)}{1 + P_s(\nu)/P_m(\nu)}, \quad (2)$$

where $P_s(\nu)$ is the Fourier transform of the sample reflection and $P_m(\nu)$ is the reference reflection from the mirror. Shen et al. recorded the chemical distribution of lactose and sucrose over the surface of a sample pellet. It was possible to distinguish the chemicals and determine the spatial distribution of the composition within the samples.

Based on these results, Cogdill et al. developed a more advanced signal processing technique for terahertz chemical mapping in real pharmaceutical tablets rather than a polyethylene matrix [99]. The tablets were direct compressed mixtures of MCC, lactose and theophylline. By using the terahertz maps of a set of calibration samples, it was possible to build different multivariate models for quantitative image analysis. The quantitative models were tested using tablets made of two spatially separated segments of different mixing ratios. No comment was made with regard to the effective sampling depth in the imaging experiments.

The first three-dimensional chemical mapping experiment using pulsed terahertz radiation was performed by Shen et al. [100]. Using the example of a flat faced model tablet that contained well-confined domains of lactose and tartaric acid the authors demonstrated how the spectral signature of the materials can be extracted non-destructively at depth (Fig. 16). A time-partitioned Fourier transform of the reflected terahertz waveform with a fixed window width was then employed to produce depth-resolved spectral components of the pulse [101]. While it was possible to extract the spectral information at depth in the sample tablet which was made of polyethylene, this material is almost transparent to terahertz radiation and thus not quite representative of a realistic pharmaceutical tablet.

In the next step, Shen and Taday demonstrated the technique in a pharmaceutical excipient matrix [102]. This paper also contains a detailed description of the technique together with the underlying theory for the pulse propagation in a multilayered sample and data on the validation of the spatial resolution at different frequencies. From their experimental results Shen and Taday conclude that, in principle, TPI provides the necessary penetration depth and specificity for non-destructive chemical mapping in a three-dimensional matrix.

The spectral resolution at depth is influenced strongly by scattering and refraction caused by the tablet matrix and further work will be necessary to develop a robust method to routinely perform three-dimensional chemical mapping experiments. First steps have been made to address this issue [103]. So far, in the experiments by Shen et al. the sample only exhibited one layer of chemical at any point over the surface of the sample. To date, no example has been

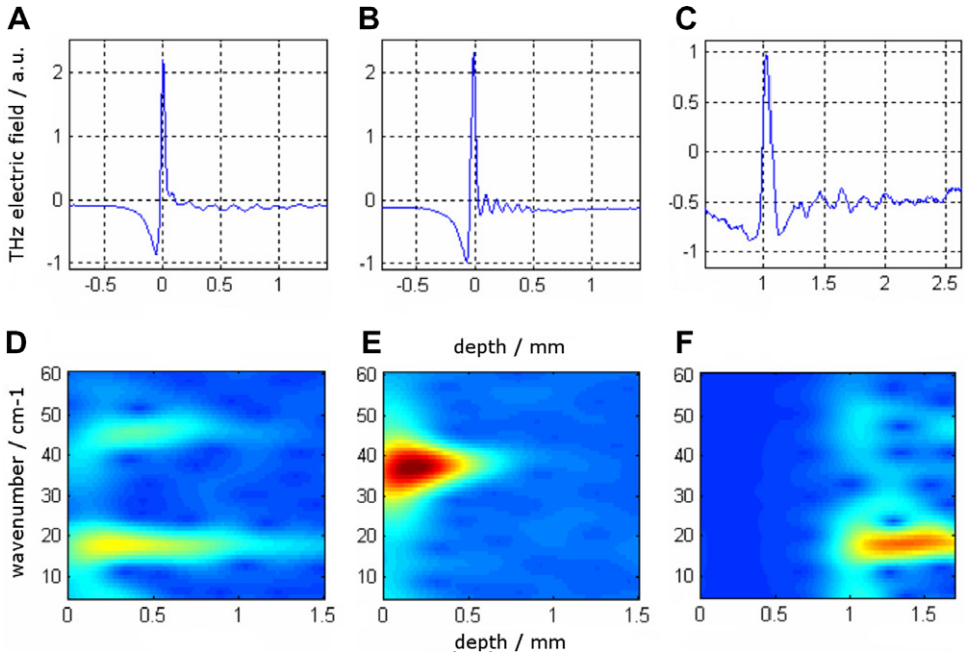

Fig. 16. Typical terahertz waveforms obtained from TPI measurement of three different areas of a sample pellet (A–C). The results of spectral content analysis of the corresponding terahertz waveforms using a time-partitioned Fourier transform are shown in (D–F), revealing the chemical signatures of lactose and tartaric acid. Note that the bright yellow regions indicate the occurrence of lactose (absorption feature at 18 cm^{-1}) and tartaric acid (absorption feature at 38 cm^{-1}). The colour scheme runs from blue (low absorbance) through yellow to red (high absorbance) (modified from [100]). (For interpretation of the references in colour in this figure legend, the reader is referred to the web version of this article.)

published of a system where a sequence of multiple or overlapping layers was spectrally resolved at depth. There are a large number of potential applications for this experiment in the context of pharmaceutical dosage forms: for example, investigating the spatial distribution of different polymorphic forms in a dosage form as a result of compaction or coating, moisture uptake during storage of a tablet, drug stability over storage time in the final product, etc.

At present, the pulsed terahertz sources are not powerful enough to image entirely through large pharmaceutical dosage forms. Attenuation due to absorption and scattering limits the range of the terahertz pulse in tablets to about 2 mm [89]. With further developments in more powerful emitters, it is quite possible that this limitation will be overcome within the next few years. With the terahertz pulse propagating through the dosage form twice in order to be detected, there is a significant interaction with the dielectric over the path length. For the future development of TPI, one challenge will be the incorporation of dispersion and diffraction effects into the data analysis. So far these effects are not accounted for and will have a strong impact on the reconstruction of the internal structure leading to distortions and increasing uncertainties at increasing depth or at interfaces with a strong curvature. For coating thicknesses below 150 μm, such as the typical film coating layer on a tablet, these effects seem negligible, however, for the resolution of internal structure in layered tablets the effects will be significant.

4.3. Transmission terahertz tomography

In analogy to tomographic experiments with X-rays as discussed in Section 2 it is possible to perform computed tomography at terahertz frequencies. To date, no example of applying this technology to pharmaceutical samples has yet been reported. The following section gives an outlook of possible future developments in this field and a discussion of the limitations in the context of pharmaceutical dosage form characterisation.

4.3.1. Pulsed setups

A good overview on tomography using pulsed terahertz systems is provided in the review by Wang and Zhang [104]. The first report of terahertz tomography by Ferguson et al. demonstrated the principle of a three-dimensional terahertz transmission tomography experiment using the example of a turkey bone fragment [105].

In contrast to the reconstruction technique outlined in Section 2.1, the frequency dependent absorption and phase shifts need to be considered for terahertz pulsed tomography. The analogous equation to Eq. S-7 in X-ray CT for terahertz tomography, gives the expression for the line integral of the parallel projection of the transmitted terahertz pulse $P(\omega,\theta,l)$ as

$$P(\omega,\theta,l) = P_t(\omega)\exp\left[\int_{(\theta,l)L}\frac{-I\omega\tilde{n}(x)}{c}\mathrm{d}x\right], \tag{3}$$

where ω is the frequency of the terahertz signal, θ, the projection angle, l the horizontal offset from the axis of rotation, L, the straight line between source and detector (see Fig. S.2A), and c, the speed of light [105]. $\tilde{n} = n + ik$ is the complex refractive index of the object along L. Here, n denotes the real refractive index and k is the extinction coefficient. The absorption coefficient α is related to the extinction coefficient as $\alpha = (2\omega k)/c$. Without going into further details on the reconstruction of these complex datasets, it is clear that this technology allows the extraction of additional information from the sample matrix. It is possible to reconstruct tomographic cross-sections that represent the attenuation of a particular frequency component or to specifically enhance the contrast between interfaces based on their differences in real refractive index. The ability to use subtle differences in the refractive index of the sample for image contrast is very powerful as demonstrated in the previous subsection on TPI.

The increase in the information content of the imaged object compared with X-ray CT due to phase sensitive detection and the use of a wide range of frequencies are significant advantages of ter-

ahertz tomography. However, the relative disadvantages are the much lower spatial resolution, strong dispersion and relatively weak light sources of terahertz CT compared to XμCT. Scattering effects in terahertz measurements also need to be fully understood and considered [103]. The data analysis is further complicated by the fact that the different frequency components in a broadband terahertz pulse have different spatial distributions in the beam profile and will, therefore, propagate through different volumes of the sample. Further research will have to explore the full potential of this technique, and address the outstanding challenges before this technique can be widely applied.

4.3.2. Terahertz quantum cascade lasers

Quantum cascade lasers (QCL) are a novel source of terahertz radiation, which can provide high power terahertz radiation either at a single frequency [106] or at multiple frequencies [107]. Rather than lasing from the bandgap transition between the conduction and valence band, a QCL is a semiconductor laser that is lasing from transitions between sub-bands. In a QCL, the conduction band is split into sub-bands by quantum confinement [108], and it is these so-called inter sub-band transitions that are used for lasing. The whole QCL device measures only a few millimetres and has the potential to be built very cheaply. Even though the development of THz-QCLs is in its early phase and the present designs require operation at temperatures below 160 K, the technology has already been employed for proof-of-principle tomographic imaging applications.

Nguyen et al. have used a THz-QCL operating at 2.9 THz combined with a Golay cell for detection in a CT setup analogous to that shown in Fig. S.1A [109]. The pulse power of the THz-QCL was 70 mW (250 ns pulse duration, 80 kHz repetition rate). The results from this approach are very promising (Fig. 17), yet it remains to be seen whether it will be possible to resolve fine internal structures of less than 1 mm. The spatial resolution of the setup is limited by the diameter of the terahertz beam.

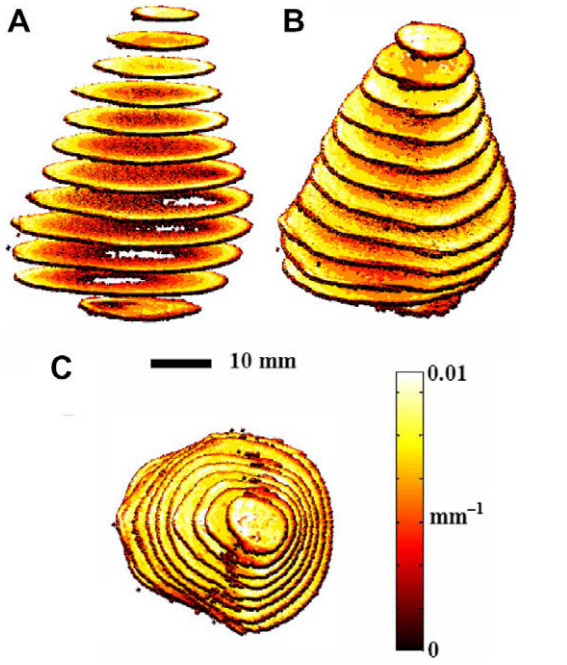

Fig. 17. Tomography of a polystyrene phantom of a head using a THz-QCL. Visualisation of the reconstructed 3D image. (A) The hole inside the phantom is revealed, (B) the shape of the phantom is reconstructed, (C) the top view shows the nose and cheek features. The data integration time was 15 min per image slice. (Reprinted with modifications from [109] with permission from the Optical Society of America).

5. Optical coherence tomography (OCT)

The development of optical coherence tomography, a contact-free non-invasive imaging technology that can be applied to both transparent and turbid media, originates from optical coherence-domain reflectometry (OCDR). OCDR is an interferometry technique, which was initially developed in order to detect defects in structures such as fibre-optic cables [110,111]. Huang et al. developed the first OCT setup and demonstrated the enormous potential of this new technology by presenting the cross-sectional images of different human tissue samples from eye and blood vessel [112].

In OCT, the radiation of a low coherence, broad bandwidth light source, such as a super-luminescent diode, is focused onto the sample object. A Michelson interferometer and an intensity detector are used to analyse the coherence of the reflected radiation. While most of the incident photons are either reflected from the surface of the sample or scattered by the sample medium, a number of photons are reflected from the internal structures of the sample. These photons still exhibit coherence and can be detected by the interferometer. Interference between the sample and the reference mirror is observed, when the optical path difference between the two arms of the interferometer is less than the coherence length of the source radiation. By scanning the reference mirror of the interferometer, depth information from the sample is obtained (Figs. 18 and 19). In analogy to TPI (Section 4.2), in OCT the axial (z) resolution is decoupled from the lateral resolution in the xy plane. The OCT measurement can be performed in the time-domain by moving the reference mirror but it is also possible to acquire the data in the frequency-domain. For frequency-domain OCT, two main configurations are in use. In both cases, the mirror is kept stationary. One method is to directly measure the spectrum at the detector, while the alternative approach is to use a narrow bandwidth light source that can be rapidly swept over a broad frequency range instead of the broad bandwidth light source. In frequency-domain OCT, significantly higher acquisition rates can be achieved with scan rates as fast as 5 MHz and no moving parts required. The acquisition speed in time-domain OCT is similar to TPI for a single point measurement. In contrast to TPI, however, 2D array detectors are available for OCT experiments, most commonly performed at near-infrared frequencies. Even though the data acquisition rates in frequency-domain OCT can be much higher than in time-domain, the measurement time is limited by the data processing time for the fast Fourier transform.

OCT is widely applied to study the microstructure of biological tissues. Depending on the tissue type, imaging depths between 1 mm and 2 cm with an axial resolution below 1 μm have been demonstrated. A review of the technology by Schmitt gives a summary of the technical aspects of OCT in biological tissues and the associated theoretical issues involved in imaging highly scattering tissues with partially coherent light [113]. Applications of OCT out-

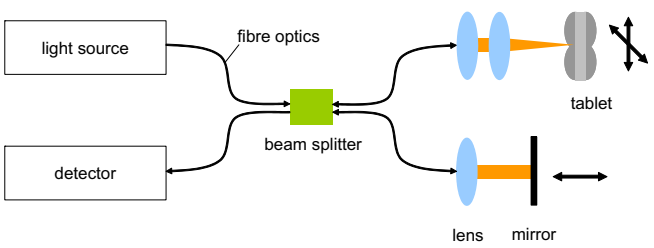

Fig. 18. Schematic of an OCT setup based on a standard fibre-optic Michelson interferometer. The mirror is scanned at each point of the sample in order to resolve the internal structure of the sample tablet in axial (z) direction. The object is imaged by mapping over the surface of the tablet. Alternatively a collimated beam together with a 2D array detector can be used to scan larger areas of the surface of the object.

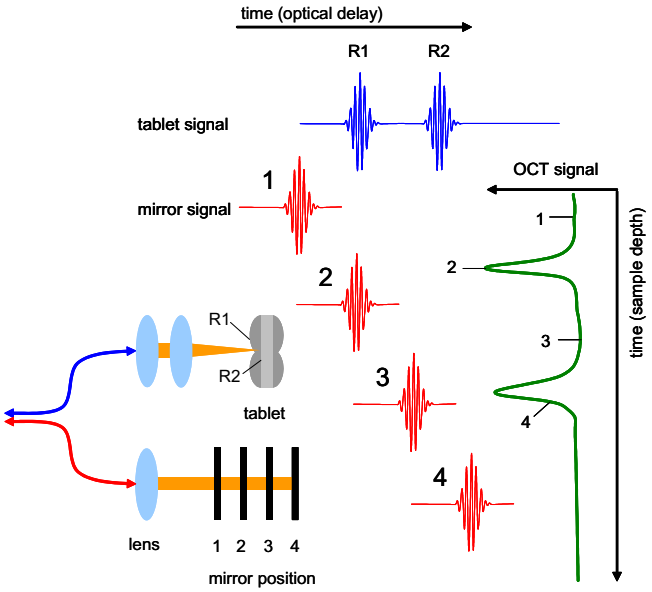

Fig. 19. Principle of an OCT measurement (an example of a setup using a pulsed light source). The schematic shows the light pulse that is reflected from the sample object (blue) and from the mirror arm of the interferometer (red). In this example two reflections of the light pulse have occurred at the internal structure of the sample object. Depending on the mirror position the two pulses travelling along the two arms of the interferometer exhibit coherence when they are united, which leads to a signal at the detector. (For interpretation of the references in colour in this figure legend, the reader is referred to the web version of this article.)

side the biomedical field have been recently reviewed by Stifter [114].

To date, there have been no reported applications of OCT in the pharmaceutical literature. However, the results of varnish layer analysis on paintings and structural characterisation of ceramics and porcelain in art conservation imply that the technology should be in principle applicable to the film coatings on pharmaceutical dosage forms as well [115–118].

Wiesauer et al. demonstrated the high axial resolution that can be achieved by more advanced OCT configurations (so-called UHR-OCT, ultra-high resolution OCT) [119]. In contrast to the standard OCT, here a Mach-Zehnder interferometer and a femtosecond laser is used rather than a Michelson interferometer and a cw source. The resolution and contrast that can be achieved on this setup were highlighted on samples of polymer film, wooden floor laminate and polymer foam (Fig. 20).

Kastner et al. have compared OCT and XμCT for applications in non-destructive materials testing [120]. The study involved a comparison of the performance to resolve the internal structures in samples of fibre reinforced materials, polymer foams, composite floor panels, multilayered foils, the geometry of complex plastic

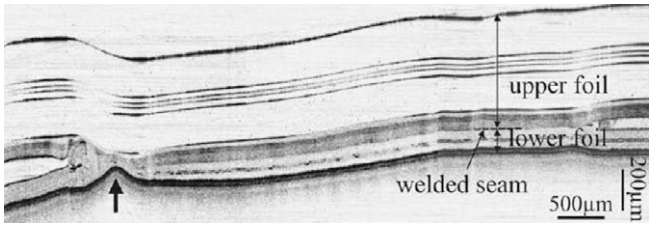

Fig. 20. OCT image of the cross-section through a polyester and polyethylene composite foil. The multiple layer structure of the composite can be clearly resolved. The arrow indicates a defect in the foil. From [119] with permission of the optical Society of America.

shapes made by injection moulding and the dimensions of very fine holes in a polyamide phantom. While both techniques are suitable to study such materials it was concluded that the advantages of OCT were its higher resolution for contact-free measurements of dimensions on surfaces of objects and in thin layers and its suitability for in-line applications in an industrial quality control context. The major advantages of XμCT were the broad range of materials that can be studied with the technique and the ability to obtain a full 3D model of the object – in contrast to OCT which, as a reflection technique, often cannot penetrate the entire object.

Compared to TPI, OCT has a potentially higher axial and lateral resolution and can achieve faster data acquisition due to the availability of array detectors at near-infrared frequencies. However, OCT measurements at near-infrared frequencies, which is the frequency range in which the current equipment is almost exclusively operating in, is problematic for imaging pharmaceutical solid dosage forms. A number of very common excipients, such as titanium dioxide, are strongly absorbing in the near-infrared and the penetration of the radiation is thus confined to the surface of the sample. In addition, the particle size of pharmaceutical formulations is often on a similar length scale as the wavelength in the near-infrared, which will lead to very strong scattering and hence reduced signal in OCT. Even though the recent work in the field of non-destructive material characterisation is encouraging and provides some indications that OCT might be useful for the characterisation of pharmaceutical solid dosage forms, further work is required in order to evaluate the potential of this technique.

6. Conclusions

Modern *in-vitro* tomography techniques can be employed to reveal unique insights into the structure and performance of pharmaceutical solid dosage forms, information which is not directly accessible by means of surface imaging techniques or measurements of bulk properties. The rich information content that can be extracted from tomographic experiments is crucial for the development of a better scientific understanding of how solid dosage forms work and how their quality and performance can be improved for optimal treatment of specific diseases and reduction of side effects. The developments in technology over the last two decades provide the scientists and engineers involved in both R&D and manufacturing with very powerful new tools that can improve the understanding and better development of robust processes to manufacture such solid dosage forms with consistent quality. All techniques are non-invasive and, with the exception of MRI when using liquids to image indirectly the solid fraction, non-destructive. This is a big leap forwards in terms of understanding what processes are going on inside a dosage form during production, storage and dissolution. It makes a lot of the, often elaborate and time-consuming techniques – that were developed in attempts to infer these properties from indirect observations or by cutting the dosage form – redundant. Nebgen et al. provide a good overview of some of these techniques in the introduction of their seminal study [46]. The information contents accessible through the four techniques introduced in this review not only span a wide range of length and timescales but also very different specificity to changes in the chemical and physical characteristics of the sample.

There is little doubt that the invention of the tablet press and the subsequent patent on the ‘pill and lozenge’ press by William Brockedon in 1843 has revolutionised the quality, stability and convenience with respect to how medicine is administered to the patient [121]. While engineers were able to transform the production process of tablets within a few decades from the compaction of simple powder mixtures by local pharmacists to fully automated

tabletting machines capable of producing up to 500 tablets per second on an industrial scale, the development of a thorough scientific understanding of the dosage form itself and how the API is released still eludes us. This difference in development of time scales is not too surprising given the already existing state of the art in compaction engineering in other industries at the time compared to the scientific understanding of the dissolution of solids which was only emerging roughly at around the same time [122–124]. Further advances in the fundamental physical chemistry of disintegration and compaction were achieved over the last century, yet the lack of experimental techniques to study such processes not only in a simple powder but also directly in tablets themselves, optically opaque compacts of often quite chemically heterogeneous particles, limited the development of a better understanding of the dosage form. While in the past this imbalance could be tolerated to a certain extent [125], the quality requirements of today's medicines and the economical costs associated with pharmaceutical production make it imperative to move on from the commonly employed empirical and indirect characterisation methods, such as weight gain during coating or the amount of released drug during dissolution testing, and to aim at achieving a full understanding of solid dosage forms through scientific first principles which in turn can provide the solid foundation for process optimisation and control. Process understanding can only be developed when both the formulation scientist and the process engineer know how changes in formulation and processing conditions impact on the performance of the end product.

Pharmaceutical solid dosage forms are complex systems, which provide a number of challenges with regards to their physical and chemical properties. In terms of physical dimensions, "[t]ablets made of compressed powders contain structure over length scales from ångstroms, the interfaces between particles and the surrounding air or water, to many micrometres, the air voids and large particles, to millimetres, the size of individual tablets". [30] The differences in length scales have a direct impact on the release characteristics of the dosage form: "For example, the rate of dissolution of the soluble component potentially depends on the dissolution rate at the interface between water and its crystalline particles; on its overall solubility and concentration-dependent diffusion constant; on any potential swelling of the insoluble matrix; as well as on structure on larger length scales, for example the porosity, which may well evolve with time" [*ibid.*]. Not only huge variations in length scales but also in time scales need to be accounted for. Modern formulations are produced with a variety of different release kinetics. The time scales of dosage form disintegration and drug release can range between a few seconds in evanescent or sublingual tablets; a few minutes in immediate release; several hours in enteric coated dosage forms, sustained or controlled release tablets; and up to several months for subcutaneous implants. There is also some preliminary evidence in the literature that even for tablets where drug release is only observed after a few hours, much more rapid processes may contribute to the performance of the dosage form. Strübing et al. for example recently observed evidence for rapid water ingress into tablets coated with a sustained-release barrier within a few minutes [126], however, the implications of this observation, which could be due to absorption of the dissolution medium into the open pore voids, are yet not understood. Apart from the challenges due to the vast range of length and time scales present, a number of changes in the physico-chemical properties of the drug and excipient molecules during processing, storage and contact with the release medium complicate the rational understanding of solid dosage forms: drug-excipient interactions, polymorphism, hydrate formation, crystallisation, supersaturation, precipitation, formation of complexes and other interactions of the drug or excipient molecules on the surface of the dosage form with molecules in the dissolution medium all have an effect on the performance of the medicine. In addition, the quality of the medicine is influenced by photo- and temperature-induced chemical degradation during storage and many other factors that can only be assessed in the final dosage form.

Quantitative experimental observations of the solid dosage form and the changes induced by contact with the dissolution medium can form the basis for the development of reproducible *in-vitro* dissolution models, which in turn would provide a robust platform for rational product development in the future. To date, a lot of knowledge is generated by understanding pure compounds and their bulk properties; however, a holistic approach that takes the whole dosage form into account is necessary to acknowledge the strong complexity on different physical and chemical levels as outlined above. The pharmaceutical scientist responsible for the formulation of the dosage form is likely to be confronted with a number of new techniques, such as the ones introduced in this review, and it is important to understand the basic physics behind tomographic techniques in order to make an adequate choice of which technique to employ, how to interpret the results and how to identify and eliminate artefacts in the measurements.

Table 1 gives an overview of the key characteristics of the different techniques.

In comparison with the other techniques, the advantages of XμCT are in the high spatial resolution that can be achieved with this technique. In addition, X-rays are able to penetrate typical pharmaceutical samples easily and are not significantly scattered or refracted. The technique is very useful to study the microstructure of, e.g. the tablet matrix and depending on the contrast of the images it can even be possible to quantify the pore size distribution. The major limitations of XμCT are due to the size restriction of the sample for high resolution measurements. Only fragments of samples with dimensions of up to $2 \cdot 2 \cdot 2\ \mathrm{mm}^3$ can be imaged at the highest resolution. An additional restriction for the measurement of large objects is that the reconstruction algorithms require the whole area of interest to be present in the field of view at any time throughout acquisition of the different projection images. This requirement makes it impossible to select small volumes of a larger object to be imaged at high resolution. However, new developments in the instrumentation now allow larger objects to be imaged at high resolution using connected scans, where the detector is moved and the field of view is extended. Such setups are able to image whole tablets for instance with an isotropic resolution of 2 μm by sequentially acquiring four connected scans, yet the acquisition time is then also four times longer than for a normal scan. The data processing and image reconstruction require substantial computational resources. Using parallel computing strategies, it is possible to process the acquired data on the time scale of a couple of hours. Besides the difficulties of imaging larger objects at high resolution, the contrast of the internal structure of solid dosage forms in XμCT is often not very strong. It is typically not possible to distinguish between API and excipient and hence the API distribution within the tablet matrix cannot be analysed. Further, the contrast between water and the tablet matrix is not very high which, together with the relatively long acquisitions times, limits the applicability of XμCT for *in situ* dissolution studies. The lack in contrast is due to the very similar electron density of the different polymers, API and water.

To date, MRI is the most established technique for the characterisation of pharmaceutical solid dosage forms of the four techniques introduced in this review. It has been mostly applied to study diffusion processes in matrix tablets, a field of research that emerged from previous applications of MRI in the materials science community to study diffusion in polymers. MRI has a unique ability to study transport processes, and it is possible to perform *in situ* imaging experiments of tablet dissolution. It has a high chemical

Table 1
Overview of the different techniques. All values are intended to give a rough estimate based on the performance of currently available instrumentation

Technique	XμCT	MRI	TPI	THz tomography	OCT
Acquisition time[4]	5-20 min ($10 \cdot 10 \cdot 10\ \mu m^3$ resolution), 20-80 min ($5 \cdot 5 \cdot 5\ \mu m^3$ resolution), 1-4 h ($2.5 \cdot 2.5 \cdot 2.5\ \mu m^3$ resolution)	5-60 min	40 min[5]	120–300 min	10 min[6]
Data processing time[7]	30-60 min ($5 \cdot 5 \cdot 5\ \mu m^3$ resolution), 480-960 min ($2.5 \cdot 2.5 \cdot 2.5\ \mu m^3$ resolution)[8]		< 1 min	1-10 min	1-10 min
Spatial resolution	$1.3 \cdot 1.3 \cdot 1.3\ \mu m^3$ [9] to $5 \cdot 5 \cdot 5\ \mu m^3$ instrument dependent	20-1000 μm[10]	$150 \cdot 150\ \mu m^2$ lateral, 30 μm axial	0.5 to 2 mm	axial $1 > z > 10\ \mu m$[11]
Maximum sample size	at maximum resolution 1-2 mm, using connected scans it is possible to image larger objects	5 mm to 30 cm[12]	21 mm	no data available	n/a[13]
Contrast mechanism	electron density	– chemical specificity to nuclei of interest (intrinsic signal) – nuclear spin relaxation times – molecular mobility	change in optical constants (mainly refractive index)	change in optical constants (mainly absorption coefficient)	change in optical constants (mainly refractive index)
Chemical sensitivity	low sensitivity due to very similar electron densities of API, excipients and water	high	high	high	low
Advantages	– high resolution – no limitations on sample geometry – geometry – high penetration power	– chemical specificity – *in situ* dissolution studies are possible – quantitative technique – ability to study flow and diffusion processes – wide range of imaging sequences is available to specifically emphasise certain properties of the sample	– strong contrast – high dynamic range – chemical sensitivity – potential for 3D chemical imaging	– strong contrast in pharmaceutically relevant excipients – imaging through entire dosage form is possible	– very fast acquisition – good spatial resolution and extremely high axial resolution – real time imaging is possible
Limitations	– long acquisition and data processing time – poor contrast between typical pharmaceutical matrix and water	– only some solids can be imaged directly; the experiments are usually destructive as they require the interaction of a liquid phase with the sample – operation of strong magnetic fields requires special safety precautions – restricted sample size in magnetic more – paramagnetic materials (such as most metals) have to be eliminated from the sample setup	– it is not possible to image through a whole tablet – scattering and refraction effects – point mapping techniques, no array detectors available yet	– experimental technique – difficult reconstruction due to scattering and diffraction effects – further developments in source and detectors technology required	– it is not possible to image through a whole tablet – strong absorption and scattering at currently available imaging frequencies (NIR)
Commercial availability	yes	yes	yes	no	yes

[4] to cover the entire volume/surface of a tablet (10 mm diameter, 5 mm thick).
[5] The acquisition time includes the time that is required to build a 3D model of the tablet. When scanning multiple tablets of the same dimensions the acquisition time for subsequent tablets is half of stated time. It is also possible to image only select areas of the tablet in much shorter time intervals.
[6] This value is an estimate, as there is no equipment on the market that is capable of automatically scanning all surfaces of the tablet.
[7] single PC workstation, dual core processor.
[8] Data processing can be performed on clusters. Algorithms are currently under development that will allow a dramatic reduction in reconstruction time down to less than 30 min at $2.5 \cdot 2.5 \cdot 2.5\ \mu m^3$ resolution.
[9] Two offset camera positions and two levels of scanning along the short axis of the object are required to achieve this resolution. The scanning and reconstruction time increase by a factor of 8 compared to $2.5 \cdot 2.5 \cdot 2.5\ \mu m^3$ resolution.
[10] the voxel size is usually not isotropic.
[11] depending on the instrument configuration; the lateral spatial resolution is diffraction limited and depends on the frequency of the light source used for the experiment.
[12] the maximum sample size is restricted by the diameter of the magnet bore and the coil used for the experiments. 89 mm refers to a typical bore in a 500 MHz system while 30 cm refers to a 85 MHz system. See Tab. S.1 for details.
[13] probe head can be applied to samples of arbitrary shape. No equipment is commercially available that can image pharmaceutical dosage forms in a fully automated fashion.

sensitivity and at the same time is able to provide spatially resolved quantitative information from within the entire volume of any dosage forms of arbitrary geometry (as long as it fits into the imaging coil). This makes MRI potentially more powerful than XμCT, which has only low chemical sensitivity, and both terahertz imaging and OCT which may struggle to provide consistent image quality throughout the volume of a dosage form. Both scattering losses or diffraction of the pulse of electromagnetic radiation used to perturb the magnetic field within the magnet, are not a problem for MRI experiments. MRI is different from other techniques in that it typically images the within aqueous phase within the dosage form rather than the solid directly. A large variety of different properties can be imaged or emphasised by making use of the different pulse sequences that have been developed. MRI is the only technique of the four that provides strong contrast between the liquid and solid phase while the dosage form is immersed in an aqueous liquid. Some of the limitations of MRI are the sample size restrictions due to the dimensions of the magnet, and the restrictions that result from the fact that no paramagnetic objects can be present in the magnet.

Compared to the other three techniques, terahertz tomography is the most recent development. Due to this disparity in development time not all aspects of the technology are fully exploited yet. The area of tomographic imaging through an entire dosage form using terahertz quantum cascade lasers is only at an experimental stage, and only preliminary feasibility studies have been performed that show the great potential for this technology for the future. However, with respect to TPI and the area of structural imaging of pharmaceutical dosage forms there is a particular reason why terahertz technology has matured much faster than the other techniques discussed here. While XμCT, MRI and OCT were all developed in other research communities and only later introduced to the characterisation of pharmaceuticals, in contrast the pharmaceutical sciences have served as the core field for the development of TPI. The role of pharmaceutics for the development of TPI is comparable to the biomedical field and the development of OCT. Commercial instrumentation that is specifically designed to image the coating structure over the whole surface of film coated tablets has been on the market for more than three years. Factors that limit the rapid development of novel applications for terahertz radiation in process research are its strong absorption by water, the need for more powerful sources, the lack of array detectors and waveguiding technology, and the limited understanding of the exact contrast mechanisms in terahertz imaging. More research is required into the fundamental physics of the interaction of terahertz radiation with matter. Effects such as strong scattering and diffraction of the radiation by the tablet matrix need to be investigated before the technology can be developed for routine tomography applications. In terms of the image acquisition speed terahertz imaging can be operated much faster than XμCT and MRI. While the strong absorption of terahertz radiation by water can be a limitation of the technique when studying processes in an entirely aqueous environment, it is very advantageous for studying the interaction of solids with liquids as it provides an excellent contrast between the two phases [127].

Of the four techniques discussed, OCT stands out in that it has not yet been applied for the characterisation of pharmaceutical solid dosage forms. However, based on the high resolution that can be achieved in the characterisation of the layer structure in plastic foil, the technique has a clear potential for future impact in the pharmaceutical field. The high axial resolution and the rapid data acquisition are the major advantages of OCT. In order to overcome the problem of strong absorption by typical pharmaceutical excipients, further developments in photonics are required to expand OCT into different frequency regimes. Most of the available instruments operate in the visible or NIR regions of the electromagnetic spectrum, where strong scattering is taking place on the length scales of pharmaceutical solids and only low penetration of the solid dosage form can be achieved. While considerable advances in scattering theory have been made in the OCT research community, the technology will benefit from sources and detectors that are able to operate at lower frequencies. The low absorption of pharmaceutical excipients at terahertz frequencies would make OCT a particularly attractive technique to bring together high resolution, high penetration and strong contrast. However, such development will be far from trivial due to the coherence length characteristics of the currently available THz-QCL and the remaining challenges for the development of more powerful detectors.

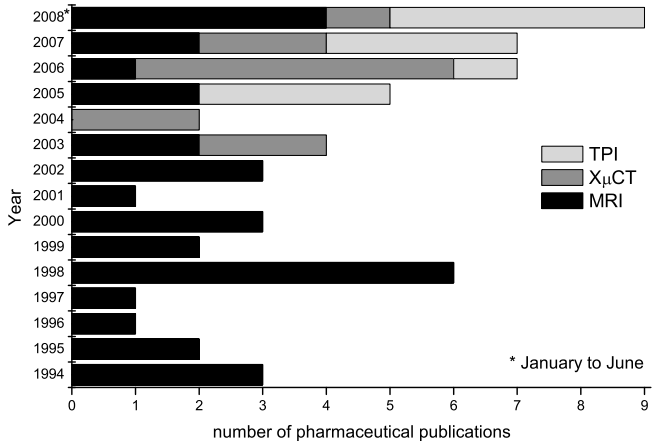

Fig. 21. Papers published on MRI, XμCT and TPI for the characterisation of pharmaceutical solid dosage forms since the first report of the application of MRI for pharmaceutical applications in 1994.

This review highlights the rapid developments in the field of tomographic imaging techniques, how such techniques have already impacted in pharmaceutical research and development and what the potential of performing non-destructive three-dimensional imaging brings into pharmaceutics. There is an increasing research activity into the characterisation of solid oral dosage forms by tomography, and the research applications diversify both in terms of what techniques are applied and which problems are explored (Fig. 21). As with all solid-state characterisation work, there is not one ideal technique to solve all problems, but we hope that this review gives a good insight into the basic working principles of the different types of tomographic approaches, and provides some rational as to which techniques to chose for a specific sample.

Acknowledgements

The authors acknowledge Ms. Gentiana Shiko and Ms. Ya Ying Chen for the help with the literature review, and both the RCUK Basic Technology Programme and Saint-Gobain plc for funding.

Appendix A. Supplementary data

Supplementary data associated with this article can be found, in the online version, at doi:10.1016/j.ejpb.2008.08.012.

References

[1] S.G. Kazarian, K.L.A. Chan, Chemical photography of drug release, Macromolecules 36 (26) (2003) 9866–9872.
[2] F. Clarke, Extracting process-related information from pharmaceutical dosage forms using near infrared microscopy, Vib. Spectrosc. 34 (1) (2004) 25–35.
[3] A.S. El-Hagrasy, H.R. Morris, F. D'Amico, R.A. Lodder, J.K. Drennen, Near-infrared spectroscopy and imaging for the monitoring of powder blend homogeneity, J. Pharm. Sci. 90 (9) (2001) 1298–1307.

[4] Y. Roggo, A. Edmond, P. Chalus, M. Ulmschneider, Infrared hyperspectral imaging for qualitative analysis of pharmaceutical solid forms, Anal. Chim. Acta 535 (1–2) (2005) 79–87.
[5] E. Rasanen, N. Sandler, Near infrared spectroscopy in the development of solid dosage forms, J. Pharm. Pharmacol. 59 (2) (2007) 147–159.
[6] J. Rantanen, Process analytical applications of Raman spectroscopy, J. Pharm. Pharmacol. 59 (2) (2007) 171–177.
[7] FDA enforcement report. Available from: <http://www.fda.gov/po/enforceindex/2007enforce.html> (accessed January 2008) (2007).
[8] A. Kak, M. Slaney, Principles of Computerized Tomographic Imaging, IEEE Press, New York, 1988.
[9] S.R. Pygall, J. Whetstone, P. Timmins, C.D. Melia, Pharmaceutical applications of confocal laser scanning microscopy: The physical characterisation of pharmaceutical systems, Adv. Drug Del. Rev. 59 (14) (2007) 1434–1452.
[10] L.A. Feldkamp, L.C. Davis, J.W. Kress, Practical cone-beam algorithm, J. Opt. Soc. Am. A Opt. Image Sci. Vis. 1 (6) (1984) 612–619.
[11] H. Barrett, W. Swindell, Radiological Imaging: The Theory of Image Formation, Detection and Processing, vol. II, Academic Press, New York, 1981.
[12] F. Natterer, The Mathematics of Computerized Tomography, Wiley, Stuttgart, 1986.
[13] J.C. Elliott, S.D. Dover, X-ray microtomography, J. Microsc. Oxf. 126 (1982) 211–213.
[14] S.R. Stock, X-ray microtomography of materials, Int. Mater. Rev. 44 (4) (1999) 141–164.
[15] B.P. Flannery, H.W. Deckman, W.G. Roberge, K.L. Damico, 3-Dimensional X-ray microtomography, Science 237 (4821) (1987) 1439–1444.
[16] G.R. Davis, J.C. Elliott, X-ray microtomography scanner using time-delay integration for elimination of ring artefacts in the reconstructed image, Nucl. Instrum. Methods Phys. Res. A Accel. Spectrom. Dect. Assoc. Equip. 394 (1–2) (1997) 157–162.
[17] G.R. Davis, J.C. Elliott, Artefacts in X-ray microtomography of materials, Mater. Sci. Technol. 22 (9) (2006) 1011–1018.
[18] N. Kozul, G.R. Davis, P. Anderson, J.C. Elliott, Elemental quantification using multiple-energy X-ray absorptiometry, Meas. Sci. Technol. 10 (3) (1999) 252–259.
[19] B.C. Hancock, M. Mullarney, X-ray microtomography of solid dosage forms, Pharm. Technol. (2005) 92–100.
[20] L. Farber, G. Tardos, J.N. Michaels, Use of X-ray tomography to study the porosity and morphology of granules, Powder Technol. 132 (1) (2003) 57–63.
[21] M.A. Ansari, F. Stepanek, Formation of hollow core granules by fluid bed in situ melt granulation: modelling and experiments, Int. J. Pharm. 321 (1–2) (2006) 108–116.
[22] C.Y. Yang, X.Y. Fu, Development and validation of a material-labeling method for powder process characterization using X-ray computed tomography, Powder Technol. 146 (1–2) (2004) 10–19.
[23] Y. Ozeki, Y. Watanabe, S. Inoue, K. Danjo, Comparison of the compression characteristics between new one-step dry-coated tablets (OSDRC) and dry-coated tablets (DC), Int. J. Pharm. 259 (1–2) (2003) 69–77.
[24] D.H. Phillips, J.J. Lannutti, Measuring physical density with X-ray computed tomography, NDT&E Int. 30 (6) (1997) 339–350.
[25] I.C. Sinka, S.F. Burch, J.H. Tweed, J.C. Cunningham, Measurement of density variations in tablets using X-ray computed tomography, Int. J. Pharm. 271 (1–2) (2004) 215–224.
[26] V. Busignies, B. Leclerc, P. Porion, P. Evesque, G. Couarraze, P. Tchoreloff, Quantitative measurements of localized density variations in cylindrical tablets using X-ray microtomography, Eur. J. Pharm. Biopharm. 64 (1) (2006) 38–50.
[27] X.W. Fu, J.A. Elliott, A.C. Bentham, B.C. Hancock, R.E. Cameron, Application of X-ray microtomography and image processing to the investigation of a compacted granular system, Part. Part. Syst. Charact. 23 (3–4) (2006) 229–236.
[28] X.W. Fu, M. Dutt, A.C. Bentham, B.C. Hancock, R.E. Cameron, J.A. Elliott, Investigation of particle packing in model pharmaceutical powders using X-ray microtomography and discrete element method, Powder Technol. 167 (3) (2006) 134–140.
[29] D. Traini, G. Loretit, A.S. Jones, P. Young, X-ray computed microtomography for the study of modified release systems, Micros. Anal. 22 (1) (2008) 13–17.
[30] E. Karakosta, P.M. Jenneson, R.P. Sear, P.J. McDonald, Observations of coarsening of air voids in a polymer-highly-soluble crystalline matrix during dissolution, Phys. Rev. E 74 (1) (2006) 011504.
[31] G. Chauve, F. Raverielle, R.H. Marchessault, Comparative imaging of a slow-release starch exciplent tablet: evidence of membrane formation, Carbohydr. Polym. 70 (1) (2007) 61–67.
[32] S.J. Inman, B.J. Briscoe, K.G. Pitt, Topographic characterization of cellulose bilayered tablets interfaces, Chem. Eng. Res. Des. 85 (A7) (2007) 1005–1012.
[33] P.C. Lauterbur, Image formation by induced local interactions: examples employing nuclear magnetic resonance, Nature 242 (5394) (1973) 190–191.
[34] P. Mansfield, P.K. Grannell, NMR diffraction in solids?, J Phys. C Solid State Phys. 6 (22) (1973) L422–L426.
[35] L.F. Gladden, M.D. Mantle, A.J. Sederman, Quantifying physics and chemistry at multiple length-scales using magnetic resonance techniques, Adv. Chem. Eng. 30 (2005) 63–135.
[36] L.F. Gladden, Nuclear-magnetic-resonance in chemical-engineering – principles and applications, Chem. Eng. Sci. 49 (20) (1994) 3339–3408.
[37] P.T. Callaghan, Principles of Nuclear Magnetic Resonance Microscopy, Clarendon, Oxford, 1991.
[38] R. Kimmich, NMR Tomography, Diffusometry, Relaxometry, Springer, Berlin, Heidelberg, 1997.
[39] C.B. Kennedy, B.J. Balcom, I.V. Mastikhin, Three-dimensional magnetic resonance imaging of rigid polymeric materials using single-point ramped imaging with T-1 enhancement (SPRITE), Can. J. Chem. Rev. Can. Chim. 76 (11) (1998) 1753–1765.
[40] M.A. Bernstein, K.F. King, X.J. Zhou (Eds.), Handbook of MRI Pulse Sequences, Academic Press, London, 2004.
[41] M.A. Bernstein, K.F. King, X.J. Zhou, Basic Pulse Sequences, in: Handbook of MRI Pulse Sequences, Academic Press, Burlington, 2004, pp. 579–647.
[42] L.F. Gladden, C. Buckley, P.S. Chow, J.F. Davidson, M.D. Mantle, A.J. Sederman, Looking into chemical products and processes, Curr. Appl. Phys. 4 (2–4) (2004) 93–97.
[43] M.D. Mantle, A.J. Sederman, Dynamic MRI in chemical process and reaction engineering, Progr. Nucl. Mag. Res. Spectr. 43 (1–2) (2003) 3–60.
[44] C.D. Melia, A.R. Rajabi-Siahboomi, R.W. Bowtell, Magnetic resonance imaging of controlled release pharmaceutical dosage forms, Pharm. Sci. Technol. Today 1 (1) (1998) 32–39.
[45] J.C. Richardson, R.W. Bowtell, K. Mader, C.D. Melia, Pharmaceutical applications of magnetic resonance imaging (MRI), Adv. Drug Del. Rev. 57 (8) (2005) 1191–1209.
[46] G. Nebgen, D. Gross, V. Lehmann, F. Muller, H-1-NMR microscopy of tablets, J. Pharm. Sci. 84 (3) (1995) 283–291.
[47] A.R. Rajabi-Siahboomi, R. Bowtell, P. Mansfield, A. Henderson, M.C. Davies, C.D. Melia, Structure and behaviour in hydrophilic matrix sustained release dosage forms: 2. NMR-imaging studies of dimensional changes in the gel layer and core of HPMC tablets undergoing hydration, J. Control. Release 31 (2) (1994) 121–128.
[48] R. Bowtell, J.C. Sharp, A. Peters, P. Mansfield, A.R. Rajabisiahboomi, M.C. Davies, C.D. Melia, NMR microscopy of hydrating hydrophilic matrix pharmaceutical tablets, Magn. Reson. Imag. 12 (2) (1994) 361–364.
[49] M. Ashraf, V.L. Iuorno, D. Coffinbeach, C.A. Evans, L.L. Augsburger, A novel nuclear-magnetic-resonance (NMR) imaging method for measuring the water front penetration rate in hydrophilic polymer matrix capsule plugs and its role in drug-release, Pharm. Res. 11 (5) (1994) 733–737.
[50] B. Madhu, J. Hjartstam, B. Soussi, Studies of the internal flow process in polymers by H-1-NMR microscopy at 500 MHz, J. Control. Release 56 (1–3) (1998) 95–104.
[51] T.M. Hyde, L.F. Gladden, R. Payne, A nuclear-magnetic-resonance imaging study of the effect of incorporating a macromolecular drug in poly(glycolic acid-co-DL-lactic acid), J. Control. Release 36 (3) (1995) 261–275.
[52] A.R. Rajabi-Siahboomi, R.W. Bowtell, P. Mansfield, M.C. Davies, C.D. Melia, Structure and behavior in hydrophilic matrix sustained release dosage forms: 4. studies of water mobility and diffusion coefficients in the gel layer of HPMC tablets using NMR imaging, Pharm. Res. 13 (3) (1996) 376–380.
[53] T.M. Hyde, L.F. Gladden, Simultaneous measurement of water and polymer concentration profiles during swelling of poly(ethylene oxide) using magnetic resonance imaging, Polymer 39 (4) (1998) 811–819.
[54] B.J. Fahie, A. Nangia, S.K. Chopra, C.A. Fyfe, H. Grondey, A. Blazek, Use of NMR imaging in the optimization of a compression-coated regulated release system, J. Control. Release 51 (2–3) (1998) 179–184.
[55] C.A. Fyfe, A.I. Blazek, Investigation of hydrogel formation from hydroxypropylmethylcellulose (HPMC) by NMR spectroscopy and NMR imaging techniques, Macromolecules 30 (20) (1997) 6230–6237.
[56] C.A. Fyfe, A.I. Blazek, Complications in investigations of the swelling of hydrogel matrices due to the presence of trapped gas, J. Control. Release 52 (1–2) (1998) 221–225.
[57] M. Kojima, S. Ando, T. Kataoka, K. Hirota, K. Aoyagi, H. Nakagami, Magnetic resonance imaging (MRI) study of swelling and water mobility in micronized low-substituted hydroxypropylcellulose matrix tablets, Chem. Pharm. Bull. 46 (2) (1998) 324–328.
[58] J.E.M. Snaar, R. Bowtell, C.D. Melia, S. Morgan, B. Narasimhan, N.A. Peppas, Self-diffusion and molecular mobility in PVA-based dissolution-controlled systems for drug delivery, Magn. Reson. Imag. 16 (5–6) (1998) 691–694.
[59] B. Narasimhan, J.E.M. Snaar, R.W. Bowtell, S. Morgan, C.D. Melia, N.A. Peppas, Magnetic resonance imaging analysis of molecular mobility during dissolution of poly(vinyl alcohol) in water, Macromolecules 32 (3) (1999) 704–710.
[60] G. Tomer, M.D. Mantle, L.F. Gladden, J.M. Newton, Measuring water distribution in extrudates using magnetic resonance imaging (MRI), Int. J. Pharm. 189 (1) (1999) 19–28.
[61] C.A. Fyfe, H. Grondey, A.I. Blazek-Welsh, S.K. Chopra, B.J. Fahie, NMR imaging investigations of drug delivery devices using a flow-through USP dissolution apparatus, J. Control. Release 68 (1) (2000) 73–83.
[62] C.A. Fyfe, A.I. Blazek-Welsh, Quantitative NMR imaging study of the mechanism of drug release from swelling hydroxypropylmethylcellulose tablets, J. Control. Release 68 (3) (2000) 313–333.
[63] S. Harding, H. Baumann, T. Gren, A. Seo, NMR microscopy of the uptake, distribution and mobility of dissolution media in small, sub-millimetre drug delivery systems, J. Control. Release 66 (1) (2000) 81–99.
[64] A. Djemai, L.F. Gladden, J. Booth, R.S. Kittlety, P.R. Gellert, MRI investigation of hydration and heterogeneous degradation of aliphatic polyesters derived from lactic and glycolic acids: a controlled drug delivery device, Magn. Reson. Imag. 19 (3–4) (2001) 521–523.
[65] J. Tritt-Goc, J. Kowalczuk, In situ real time observation of the disintegration of paracetamol tablets in aqueous solution by magnetic resonance imaging, Eur. J. Pharm. Sci. 15 (4) (2002) 341–346.

[66] W.E. Baille, C. Malveau, X.X. Zhu, R.H. Marchessault, NMR imaging of high-amylose starch tablets. 1. Swelling and water uptake, Biomacromolecules 3 (1) (2002) 214–218.
[67] C. Malveau, W.E. Baille, X.X. Zhu, R.H. Marchessault, NMR imaging of high-amylose starch tablets. 2. Effect of tablet size, Biomacromolecules 3 (6) (2002) 1249–1254.
[68] J.C.D. Sutch, A.C. Ross, W. Kockenberger, R.W. Bowtell, R.J. MacRae, H.N.E. Stevens, C.D. Melia, Investigating the coating-dependent release mechanism of a pulsatile capsule using NMR microscopy, J. Control. Release 92 (3) (2003) 341–347.
[69] M.L. Johns, L.F. Gladden, Magnetic resonance studies of dissolving particulate solids, Magn. Reson. Imag. 21 (3–4) (2003) 395–396.
[70] S. Baumgartner, G. Lahajnar, A. Sepe, J. Kristl, Quantitative evaluation of polymer concentration profile during swelling of hydrophilic matrix tablets using H-1 NMR and MRI methods, Eur. J. Pharm. Biopharm. 59 (2) (2005) 299–306.
[71] H. Therien-Aubin, W.E. Baille, X.X. Zhu, R.H. Marchessault, Imaging of high-amylose starch tablets. 3. Initial diffusion and temperature effects, Biomacromolecules 6 (6) (2005) 3367–3372.
[72] A. Djemai, I.C. Sinka, NMR imaging of density distributions in tablets, Int. J. Pharm. 319 (1–2) (2006) 55–62.
[73] E. Karakosta, P.J. McDonald, An MRI analysis of the dissolution of a soluble drug incorporated within an insoluble polymer tablet, Appl. Magn. Reson. 32 (1–2) (2007) 75–91.
[74] J.H.P. Collins, L.F. Gladden, I.J. Hardy, M.D. Mantle, Characterizing the evolution of porosity during controlled drug release, Appl. Magn. Reson. 32 (1–2) (2007) 185–204.
[75] H. Therien-Aubin, X.X. Zhu, F. Ravenelle, R.H. Marchessault, Membrane formation and drug loading effects in high amylose starch tablets studied by NMR imaging, Biomacromolecules 9 (4) (2008) 1248–1254.
[76] V. Busignies, P. Porion, B. Leclerc, P. Evesque, P. Tchoreloff, Application of PGSTE-NMR technique to characterize the porous structure of pharmaceutical tablets, Eur. J. Pharm. Biopharm. (2008), doi:10.1016/j.ejpb.2008.02.008.
[77] S. Strübing, T. Abboud, R.V. Contri, H. Metz, K. Mäder, New insights on poly(vinyl acetate)-based coated floating tablets: Characterisation of hydration and CO2 generation by benchtop MRI and its relation to drug release and floating strength, Eur. J. Pharm. Biopharm. 69 (2) (2008) 708–717.
[78] P. Kulinowski, P. Dorozynski, R. Jachowicz, W.R. Weglarz, Integrated system for dissolution studies and magnetic resonance imaging of the controlled release, polymer-based dosage forms – a tool for quantitative assessment of hydrogel formation processes, J. Pharm. Biomed. Anal. (2008), doi:10.1016/j.jpba.2008.06.025.
[79] M. Ilg, Neue Anwendungen der NMR Bildgebung in Chemie und Biologie, Ph.D. Thesis, University of Tübingen, 1990. (Some previous work on MRI of coated delayed-release tablets has been reported in the Ph.D. thesis of M. Ilg, but this work was not published in the pharmaceutical literature).
[80] D.H. Auston, K.P. Cheung, Coherent time-domain far-infrared spectroscopy, J. Opt. Soc. Am. B 2 (4) (1985) 606.
[81] C. Fattinger, D. Grischkowsky, Terahertz beams, Appl. Phys. Lett. 54 (6) (1989) 490–492.
[82] M.F. Kimmitt, Restrahlen to T-rays – 100 years of terahertz radiation, J. Biol. Phys. 29 (2) (2003) 77–85.
[83] J.A. Zeitler, P.F. Taday, D.A. Newnham, M. Pepper, K.C. Gordon, T. Rades, Terahertz pulsed spectroscopy and imaging in the pharmaceutical setting – a review, J. Pharm. Pharmacol. 59 (2) (2007) 209–223.
[84] J.A. Zeitler, T. Rades, P. Taday, Pharmaceutical and security applications of terahertz spectroscopy, in: S. Dexheimer (Ed.), THz Spectroscopy: Principles and Applications, CRC Press, Boca Raton, FL, 2007, pp. 299–323.
[85] G.M. Day, J.A. Zeitler, W. Jones, T. Rades, P.F. Taday, Understanding the influence of polymorphism on phonon spectra: lattice dynamics calculations and terahertz spectroscopy of carbamazepine, J. Phys. Chem. B 110 (1) (2006) 447–456.
[86] J.A. Zeitler, P. Taday, K. Gordon, M. Pepper, T. Rades, Solid-state transition mechanism in carbamazepine polymorphs by time-resolved terahertz spectroscopy, ChemPhysChem 8 (13) (2007) 1924–1927.
[87] J.A. Zeitler, P. Taday, M. Pepper, T. Rades, Relaxation and crystallization of amorphous carbamazepine studied by terahertz pulsed spectroscopy, J. Pharm. Sci. 96 (10) (2007) 2703–2709.
[88] W.L. Chan, J. Deibel, D.M. Mittleman, Imaging with terahertz radiation, Rep. Prog. Phys. 70 (8) (2007) 1325.
[89] J.A. Zeitler, Y.C. Shen, C. Baker, P.F. Taday, M. Pepper, T. Rades, Analysis of coating thickness, structure and uniformity in solid oral dosage forms by 3D terahertz pulsed imaging, J. Pharm. Sci. 96 (2) (2007) 330–340.
[90] D.M. Mittleman, S. Hunsche, L. Boivin, M.C. Nuss, T-ray tomography, Opt. Lett. 22 (12) (1997) 904–906.
[91] A.J. Fitzgerald, B.E. Cole, P.F. Taday, Nondestructive analysis of tablet coating thicknesses using terahertz pulsed imaging, J. Pharm. Sci. 94 (1) (2005) 177–183.
[92] L. Ho, R. Müller, M. Römer, K.C. Gordon, J. Heinämäki, P. Kleinebudde, M. Pepper, T. Rades, Y. Shen, C.J. Strachan, P. Taday, J.A. Zeitler, Analysis of sustained-release tablet film coats using terahertz pulsed imaging, J. Control. Release 119 (3) (2007) 253–261.
[93] J.A. Spencer, Z. Gao, T. Moore, L.F. Buhse, P.F. Taday, D.A. Newnham, Y. Shen, A. Portieri, A. Husain, Delayed release tablet dissolution related to coating thickness by terahertz pulsed image mapping, J. Pharm. Sci. 97 (4) (2008) 1543–1550.
[94] L. Ho, R. Müller, K.C. Gordon, P. Kleinebudde, M. Pepper, T. Rades, Y. Shen, P.F. Taday, J.A. Zeitler, Applications of terahertz pulsed imaging to sustained-release tablet film coating quality assessment and dissolution performance, J. Control. Release 127 (1) (2008) 79–87.
[95] M. Pore, J.A. Zeitler, S. Ngai, P.F. Taday, C. Cooney, Application of terahertz pulsed spectroscopy for evaluation of properties of pharmaceutical tablets, in: Pittcon, The Pittsburgh Conference, Chicago, USA, 2007.
[96] R. Palermo, R.P. Cogdill, S.M. Short, J.K. Drennen III, P.F. Taday, Density mapping and chemical component calibration development of four-component compacts via terahertz pulsed imaging, J. Pharm. Biomed. Anal. 46 (1) (2008) 36–44.
[97] L. Ho, R. Müller, K.C. Gordon, P. Kleinebudde, M. Pepper, T. Rades, Y. Shen, P.F. Taday, J.A. Zeitler, Terahertz pulsed imaging as an analytical tool for sustained-release tablet film coating, Eur. J. Pharm. Biopharm. (2009), doi:10.1016/j.ejpb.2008.06.023.
[98] Y.C. Shen, P.F. Taday, D.A. Newnham, M. Pepper, Chemical mapping using reflection terahertz pulsed imaging, Semicond. Sci. Technol. 20 (7) (2005) S254–S257.
[99] R.P. Cogdill, S.M. Short, R. Forcht, Z. Shi, Y. Shen, P. Taday, C.A. Anderson, J.K. Drennen, An efficient method-development strategy for quantitative chemical imaging using terahertz pulse spectroscopy, J. Pharm. Innov. 1 (1) (2006) 63–75.
[100] Y.C. Shen, P.F. Taday, D.A. Newnham, M.C. Kemp, M. Pepper, 3D chemical mapping using terahertz pulsed imaging, in: R.J. Hwu, K.J. Linden (Eds.), Terahertz and Gigahertz Electronics and Photonics IV, vol. 5727, SPIE, San Jose, CA, USA, 2005, pp. 24–31.
[101] Y.C. Shen, P.C. Upadhya, E.H. Linfield, H.E. Beere, A.G. Davies, Terahertz generation from coherent optical phonons in a biased GaAs photoconductive emitter, Phys. Rev. B 69 (23) (2004) 235325.
[102] Y.C. Shen, P.F. Taday, Development and application of terahertz pulsed imaging for nondestructive inspection of pharmaceutical tablet, IEEE J. Sel. Top. Quantum Electron. 14 (2) (2008) 407–415.
[103] Y.C. Shen, P.F. Taday, M. Pepper, Elimination of scattering effects in spectral measurement of granulated materials using terahertz pulsed spectroscopy, Appl. Phys. Lett. 92 (5) (2008) 051103.
[104] S. Wang, X.C. Zhang, Pulsed terahertz tomography, J. Phys. D Appl. Phys. 37 (4) (2004) R1–R36.
[105] B. Ferguson, S.H. Wang, D. Gray, D. Abbot, X.C. Zhang, T-ray computed tomography, Opt. Lett. 27 (15) (2002) 1312–1314.
[106] R. Kohler, A. Tredicucci, F. Beltram, H.E. Beere, E.H. Linfield, A.G. Davies, D.A. Ritchie, R.C. Iotti, F. Rossi, Terahertz semiconductor-heterostructure laser, Nature 417 (6885) (2002) 156–159.
[107] G. Scalari, C. Walther, J. Faist, H. Beere, D. Ritchie, Electrically switchable, two-color quantum cascade laser emitting at 1.39 and 2.3 THz, Appl. Phys. Lett. 88 (14) (2006) 141102.
[108] J. Faist, F. Capasso, D.L. Sivco, C. Sirtori, A.L. Hutchinson, A.Y. Cho, Quantum cascade laser, Science 264 (5158) (1994) 553–556.
[109] K.L. Nguyen, M.L. Johns, L.F. Gladden, C.H. Worrall, P. Alexander, H.E. Beere, M. Pepper, D.A. Ritchie, J. Alton, S. Barbieri, E.H. Linfield, Three-dimensional imaging with a terahertz quantum cascade laser, Opt. Expr. 14 (6) (2006) 2123–2129.
[110] R.C. Youngquist, S. Carr, D.E.N. Davies, Optical coherence-domain reflectometry – a new optical evaluation technique, Opt. Lett. 12 (3) (1987) 158–160.
[111] K. Takada, I. Yokohama, K. Chida, J. Noda, New measurement system for fault location in optical wave-guide devices based on an interferometric-technique, Appl. Opt. 26 (9) (1987) 1603–1606.
[112] D. Huang, E.A. Swanson, C.P. Lin, J.S. Schuman, W.G. Stinson, W. Chang, M.R. Hee, T. Flotte, K. Gregory, C.A. Puliafito, J.G. Fujimoto, Optical coherence tomography, Science 254 (5035) (1991) 1178–1181.
[113] J.M. Schmitt, Optical coherence tomography (OCT): a review, IEEE J. Sel. Top. Quantum Electron. 5 (4) (1999) 1205–1215.
[114] D. Stifter, Beyond biomedicine: a review of alternative applications and developments for optical coherence tomography, Appl. Phys. B Lasers Opt. 88 (3) (2007) 337–357.
[115] P. Targowski, B. Rouba, M. Wojtkowski, A. Kowalczyk, The application of optical coherence tomography to non-destructive examination of museum objects, Stud. Conserv. 49 (2) (2004) 107–114.
[116] H. Liang, M.G. Cid, R.G. Cucu, G.M. Dobre, A.G. Podoleanu, J. Pedro, D. Saunders, En-face optical coherence tomography – a novel application of non-invasive imaging to art conservation, Opt. Expr. 13 (16) (2005) 6133–6144.
[117] T. Arecchi, M. Bellini, C. Corsi, R. Fontana, M. Materazzi, L. Pezzati, A. Tortora, A new tool for painting diagnostics: optical coherence tomography, Opt. Spectrosc. 101 (1) (2006) 23–26.
[118] D.C. Adler, J. Stenger, I. Gorczynska, H. Lie, T. Hensick, R. Spronk, S. Wolohojian, N. Khandekar, J.Y. Jiang, S. Barry, A.E. Cable, R. Huber, J.G. Fujimoto, Comparison of three-dimensional optical coherence tomography and high resolution photography for art conservation studies, Opt. Expr. 15 (24) (2007) 15972–15986.
[119] K. Wiesauer, M. Pircher, E. Götzinger, S. Bauer, R. Engelke, G. Ahrens, G. Grützner, C. Hitzenberger, D. Stifter, En-face scanning optical coherence tomography with ultra-high resolution for material investigation, Opt. Expr. 13 (3) (2005) 1015–1024.
[120] J. Kastner, E. Schlotthauer, E. Breuer, K. Wiesauer, D. Stifter, Optische Kohärenztomografie und 3D-Röntgen-Computertomografie, MP Mater. Test. (4) (2007) 177–183.

[121] L.F. Kebler, The tablet industry – its evolution and present status. the composition of tablets and methods of analysis, J. Am. Pharm. Assoc. 3 (1914) 820–848, 937–958, 1062–1099.
[122] A. Fick, About diffusion, Phil. Mag. 10 (4) (1855) 30–39.
[123] A.A. Noyes, W.R. Whitney, The rate of solution of solid substances in their own solutions, J. Am. Chem. Soc. 19 (12) (1897) 930–934.
[124] A. Einstein, Über die von der Molekularkinetischen Theorie der Wärme geforderte Bewegung von in ruhenden Flüssigkeiten suspendierten Teilchen, Ann. D. Phys. 322 (8) (1905) 549–560.
[125] L. Aboud, S. Henry, New prescription for drug makers: update the plants, Wall Street J. (2003) A.1.
[126] S. Strubing, H. Metz, K. Mader, Mechanistic analysis of drug release from tablets with membrane controlled drug delivery, Eur. J. Pharm. Biopharm. 66 (1) (2007) 113–119.
[127] J. Obradovic, J.H.P. Collins, O. Hirsch, M.D. Mantle, M.L. Johns, L.F. Gladden, The use of thz time-domain reflection measurements to investigate solvent diffusion in polymers, Polymer 48 (12) (2007) 3494–3503.